PAPER • OPEN ACCESS

Tunable optical metasurfaces enabled by chalcogenide phase-change materials: from the visible to the THz

To cite this article: C Ruiz de Galarreta *et al* 2020 *J. Opt.* **22** 114001

View the article online for updates and enhancements.

Tunable optical metasurfaces enabled by chalcogenide phase-change materials: from the visible to the THz

C Ruiz de Galarreta[1], S G-C Carrillo[1], Y-Y Au[1], E Gemo[1], L Trimby[1], J Shields[1], E Humphreys[1], J Faneca[1], L Cai[1,2], A Baldycheva[1], J Bertolotti[1] and C D Wright[1]

[1] College of Engineering, Mathematics and Physical Sciences, University of Exeter, Exeter EX4 4QF, United Kingdom
[2] State Key Laboratory of Modern Optical Instrumentation, College of Optical Science and Engineering, Zhejiang University, Hangzhou 310027, People's Republic of China

E-mail: david.wright@exeter.ac.uk

Abstract
Metasurfaces and nanoantennas are redefining what can be achieved in terms of optical beam manipulation, as they provide a versatile design platform towards moulding the flow of light at will. Yet, once a conventional metasurface is designed and realised, its effect on optical beams is repeatable and stationary, thus its performance is 'locked-in' at the fabrication stage. A much wider range of applications, such as dynamic beam steering, reconfigurable and dynamic lensing, optical modulation and reconfigurable spectral filtering, could be achieved if real-time tuning of metasurface optical properties were possible. Chalcogenide phase-change materials, because of their rather unique ability to undergo abrupt, repeatable and non-volatile changes in optical properties when switched between their amorphous and crystalline phases, have in recent years been combined with metasurface architectures to provide a promising platform for the achievement of dynamic tunability. In this paper, the concept of dynamically tunable phase-change metasurfaces is introduced, and recent results spanning the electromagnetic spectrum from the visible right through to the THz regime are presented and discussed. The progress, potential applications, and possible future perspectives of phase-change metasurface technology are highlighted, and requirements for the successful implementation of real-world applications are discussed.

Keywords: Phase-change materials, phase-change metasurfaces, tunable metasurfaces, reconfigurable nanoantennas, reconfigurable integrated photonics

(Some figures may appear in colour only in the online journal)

1. Introduction

The ability to control the spatio-temporal nature of light has been pursued by the human race almost since the beginning of mankind. Traditional bulky optics such as lenses, mirrors or filters have been employed for this purpose for hundreds of years, and are still today key components for focusing, imaging, attenuating and redirecting light in most of our modern optical systems and devices [1]. However, classical optical components suffer from unavoidable limitations in terms of size, weight or spatial/spectral resolution [2]. A new and more flexible approach to light manipulation emerged nearly two decades ago, with the introduction of optical nanoantennas and metasurfaces [3–5]. Such devices are engineered

structures consisting of sub-wavelength building blocks either periodically or randomly arranged [5, 6]. By properly engineering the spacing, dimensions and electromagnetic properties of such building blocks (named meta-atoms or nanoantennas), optical metasurfaces can achieve sub-wavelength local amplitude, phase and polarisation control of light, and thus mimic, and even outperform, the functionalities of conventional optics without the need of bulky components and systems [4, 6]. Metasurfaces achieve this by engineering the interaction between their meta-atoms and electromagnetic (EM) waves to induce localised resonances, that in turn lead to abrupt amplitude and phase gradients [4, 6]. Hence, optical metasurfaces can be employed to provide arbitrary control of reflected and/or transmitted waves, paving the way to the development of a new class of compact photonic 'meta-devices' with novel and exotic functionalities, including super absorbers, frequency selective surfaces/switches, anomalous reflection/refraction for beam steering, flat lensing, vortex beam generators, holographic displays and much more [7].

Despite optical metasurfaces having emerged as a versatile platform that can offer clear advantages over classical optical components, the performance of conventional approaches is nevertheless fixed by design, and thus locked-in at the fabrication stage. That is, their electromagnetic properties are static, so that a particular metasurface will have a repeatable and stationary effect on optical beams. A wider range of applications (such as dynamic beam steering or lensing, tunable optical switching or filtering, tunable polarisation and much more) could be achieved if dynamic tuning of the metasurface optical properties were possible. Motivated by this fact, in recent years several approaches to reconfigurable and dynamically tunable (or 'active') metasurfaces have been proposed [8–28]. As summarised in figure 1, to date five principal methods have been suggested for this purpose, including optically, electrically, thermally, chemically and mechanically tunable metasurfaces [9]. Excluding the last case (which is based on actively changing the geometrical design parameters using microelectromechanical systems and/or flexible substrates [10, 11]), the remaining methodologies, discussed briefly below, are based on modifying the optical properties (refractive indices) of the metasurface constituent materials, to introduce changes in its electromagnetic performance.

In the case of optically tunable metasurfaces, tuning of the refractive index is generally achieved by means of non-linear optical effects driven by ultrafast, high power laser irradiation [9, 12]. This includes photo-carrier injection and optical Kerr or two-photon effects, induced in metasurfaces made of semiconductors or metals such as Si, Ge or Au [12–14]. Due to the ultrafast nature of such physical processes (i.e. typically the picosecond timescale or faster) [12], non-linear optical tuning provides, among the rest of available methodologies, the quickest tuning effects, but in turn tunability cannot be maintained for long periods due to short relaxation times [12, 14].

Electrically tunable metasurfaces can be considered as the electrical counterpart to optical tuning, as their operation is based on changing the optical properties of the metasurface constituent materials, but via electrical stimuli. Such
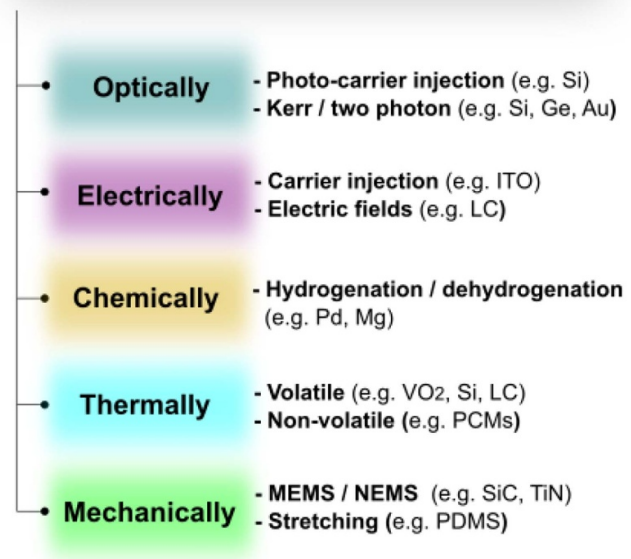

Figure 1. Methods currently employed for the development of tunable optical metasurfaces and nanoantennas.

stimuli are naturally slower than non-linear optical processes (typically on the nanosecond timescale or longer), but in turn can be maintained over time [9, 15–18]. Metasurfaces of this form are typically made of meta-atoms formed by electrically sensitive materials. This includes, for instance, the use of liquid crystals (LCs), indium tin oxide (ITO) or 2D materials, whose refractive indices can be selectively modified via electric field induced molecular re-orientations (in LCs) or electrical carrier injection (in ITO and 2D materials) [9, 15–18].

Chemically tunable metasurfaces are based on the use of chemically sensitive materials as building blocks, where the refractive index can be altered via chemical reactions such as hydrogenation-dehydrogenation processes in the case of palladium and magnesium based metasurfaces [19, 20].

Finally, thermal tuning of metasurfaces arises from the combination of optical metasurfaces with materials whose dielectric properties are thermally sensitive [9, 21–25]. In this context, thermal tuning can be subdivided in two groups depending on their underlying mechanism: volatile and non-volatile tuning. The former requires a constant heat stimulus to hold changes of the dielectric function over time, and takes advantage of materials with sizeable temperature-dependent permittivities, such as volatile phase-transition materials (e.g. VO_2 [21, 22]), or thermotropic LC [23, 24] and semiconductors (e.g. Si or Ge [25]). On the contrary, non-volatile thermal tuning does not require a constant heat stimulus, and is currently mainly based on the use of chalcogenide phase change materials (PCMs), typically made of alloys containing Ge, Sb and Te [29, 30]. PCMs exhibit dramatic differences in optical properties between their crystalline and amorphous states, and can be switched between those states quickly and repeatedly.

Moreover, both states are stable for extremely long durations (years) at room temperature [29, 30].

Both volatile and non-volatile thermal switching can be successfully carried out in tunable metasufaces employing a variety of heating mechanisms, such as direct electrical switching (e.g. by passing a current through chalcogenide materials), by indirect electrical switching (i.e. by embedding resistive micro-heaters into the metasurface structure [26], by optical heating via laser excitation [27], or simply via direct hot plate annealing [28] (with this last method only suitable for lab-based characterisations, not device applications).

Within the above-described methodologies, thermal tuning employing chalcogenide phase-change materials is arguably one of the most explored approaches to yield dynamically tunable metasurfaces and thin films [27, 28, 30–44]. This is mainly due to the rather unique physical properties exhibited by chalcogenide PCMs alloys. That is, the large contrast in refractive index between their amorphous and crystalline states, non-volatility, fast switching times (sub-nanosecond), and large number of switching cycles (up to 10^{15} or more) [45]. Such properties could potentially result in photonic metadevices having high optical contrast, low power consumption, high operational speed and large endurance [29, 30]. In addition, PCM thin film deposition processes such as magnetron sputtering [26, 41], pulsed laser deposition [46] or chemical vapour depostion and atomic layer deposition [47] are well-stablished, and optical memories based on the use of PCM thin films have been commercially available for several decades [29]. Similarly, the fabrication methods for PCM metasurfaces are well established, and take advantage of fairly standard e-beam or optical lithography and lift-off and/or wet/-plasma etching techniques [27, 28, 30, 35–42]. Lithography-free, laser-induced fabrication of PCM metadevices via direct structuring/crystallisation of PCM blanket films is also possible, as demonstrated in [48] for the provision of reconfigurable metasurfaces and Fresnel zone plates. Indeed, the last few years have seen the development of a wide range of PCM-based active metasurface prototypes, spanning from the visible to the THz spectrum and including tunable structural colour generators [37], active beam steering and lensing [27], active polarisation conversion [32, 40], reconfigurable super absorbers/modulators [41, 42], band-pass filters [43] and much more [44].

Due to the outstanding physical properties of phase-change materials, interest in the field of reconfigurable phase-change metasurfaces is growing fast (see for example recent interesting reviews [30, 49, 50]). Here we highlight the recent progress, applications and technological challenges of dynamically tunable phase-change material based metasurfaces across the electromagnetic spectrum, going from the visible to the THz regime. In section 2, we begin with a description of the most relevant physical properties of traditionally employed chalcogenide phase-change materials, also highlighting the recent emergence of novel PCM compositions with enhanced optical properties. Then, the design and operation of a variety of recently reported tunable phase-change metasurfaces with promising potential applications is explored. More specifically, section 3 describes devices for reconfigurable

amplitude control in the visible spectrum, with a particular focus on tunable colour generation. In section 4, we highlight the recent progress and applications arising from both tunable amplitude and phase control of NIR radiation employing both (free-space) phase-change metasurfaces, and phase-change (on-chip) integrated photonics. Section 5 highlights the newest work carried out on reconfigurable amplitude and phase control of mid and long-wave infrared radiation employing phase-change metasurfaces. Finally, section 6 introduces the very first work carried out in the THz regime, which has emerged only over the last year or so. The paper concludes with an analysis of the current and future challenges for phase-change metasurface technologies, as well as with a discussion of their potential solutions towards their implementation in real-world applications.

2. Phase-change materials: properties and emerging applications

PCMs have been used for several decades in devices for non-volatile data storage, such as re-writable optical disks or electrical memories [29, 30, 51]. Such a non-volatile storage concept is based on their remarkable ability to switch quickly between amorphous and crystalline states via appropriate stimuli, as well as to retain the required structural phase at room temperature, even for decades. In addition, the amorphous-to-crystalline transition comes with dramatic changes in electro-optical properties, which can be of near a factor of three difference in the refractive index, and up to five orders of magnitude change in electrical resistivity, depending on the PCM compound [29, 30]. Such an outstanding contrast can be indeed appreciated in figure 2(a), where the refractive index n and extinction coefficient k of the archetypal PCM alloy $Ge_2Sb_2Te_5$ (GST225) is shown from the visible (VIS) to the infrared (IR).

PCMs invariably contain elements (usually Te, but also sometimes S and Se) from Group VIA—the chalcogens—of the periodic table, hence the name 'chalcogenides'. Among the chalcogenide PCMs, the ternary compound $Ge_2Sb_2Te_5$ is undoubtedly the most widely used, and is often known as the 'archetypal', PCM. $Ge_2Sb_2Te_5$ is a semiconductor whose amorphous phase is typically characterised by having high electrical resistivity, as well as low optical losses at frequencies below its bandgap energy, the latter being typically around 0.7 to 0.8 eV [53]. Crystallisation results in a shift of the bandgap towards lower energies (0.5–0.6 eV), thus a higher optical loss, lower resistivity state [29, 30, 53, 54]. Crystalline $Ge_2Sb_2Te_5$ exists in two phases, the lowest energy form of which has a hexagonal close packed (hcp) structure [54]. However, in memory and related applications where the material is switched rapidly into the crystal state, the crystal phase that is formed is invariably the metastable (distorted) face-centred-cubic (fcc) structure [29, 54]. Since, under appropriate excitation conditions (see later) crystallisation can be achieved very quickly indeed (nanoseconds or less, see e.g. [54–58]) it is reasonable to assume that the atomic positions remain similar
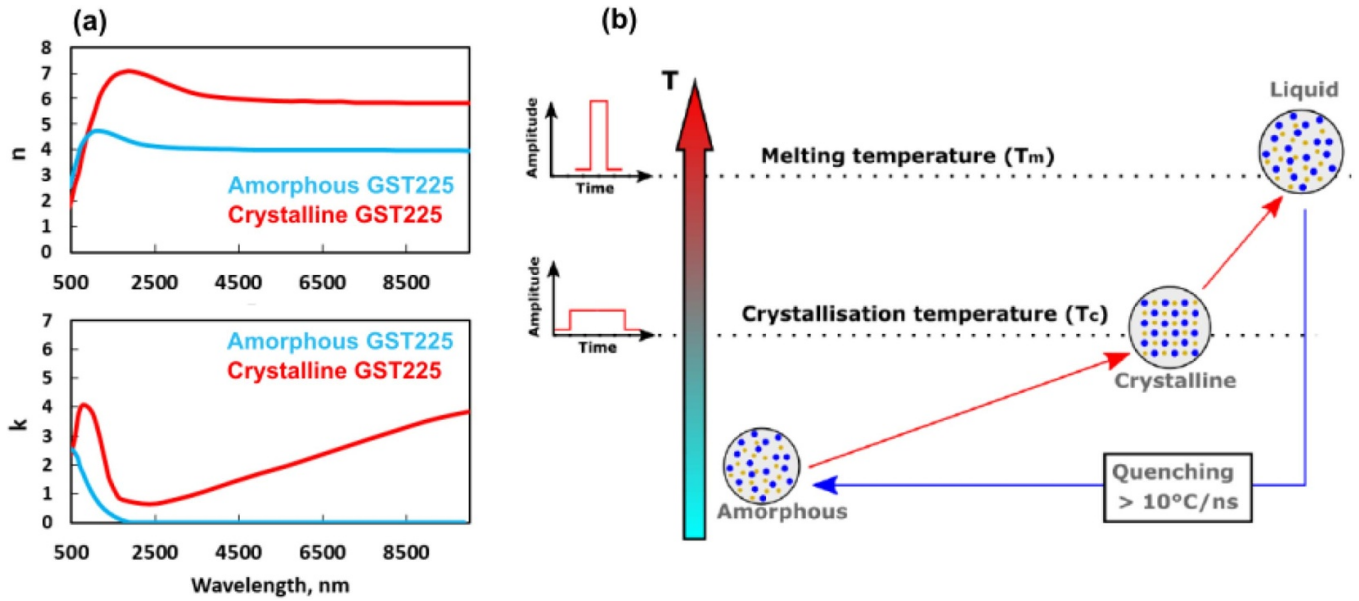
Figure 2. (a) Refractive index *n* (top) and extinction coefficient *k* (bottom) of the well-known PCM compound, $Ge_2Sb_2Te_5$ or GST225 for both amorphous and crystalline states. (b) Schematics showing optimum crystallisation and re-amorphisation conditions for a successful phase-change transition. Data shown in (a) were extracted from [52].

on switching between phases, and that the phase transition occurs without significant atomic diffusion. For a more detailed discussion of such the basic physical properties of $Ge_2Sb_2Te_5$, and of PCMs in general, the reader is referred to the many excellent reviews and specialist books that cover such topics, e.g. [29, 54, 59–61].

As summarised in figure 2(b), reversible switching between amorphous and crystal phases in PCMs is typically induced employing appropriate heat stimuli in the form of either optical or electrical pulses having appropriate amplitudes and durations. The amorphous-to-crystalline phase transition is driven by (relatively) long duration, low amplitude pulses to heat the material to a temperature conducive to fast crystallisation (i.e. a temperature where crystal nucleation and/or growth rates are at a maximum, typically around 400°C for $Ge_2Sb_2Te_5$ [57]). Amorphisation is achieved by heating the PCM above its melting temperature T_m (630 °C for $Ge_2Sb_2Te_5$), and cooling very rapidly (on the order of tens of °C/ns [29]) to avoid re-crystallisation; this is usually achieved using (relatively) high power, short duration excitation pulses having fast trailing edges [29, 30, 55]. Typical pulse durations used in PCM memory applications are in the tens to hundreds of nanosecond regime [54, 61], with crystallisation rate being the limiting speed factor (since the amorphisation is inherently a fast process). Sub-nanosecond electrical switching has been achieved in electrical PCM memory devices by careful design to control/maximise crystal nucleation and growth rates [61], and optical switching with picosecond and femtosecond excitation pulses has also been demonstrated (though with crystallisation taking several nanoseconds to complete, see e.g. [55, 56]).

In addition, intermediate states (i.e. between full amorphous and fully crystalline phases) are also achievable via partial crystallisation or partial re-amorphization of the material,

using appropriate excitation pulses. Indeed, the writing and reading of 16 intermediate levels has already been reliably demonstrated in electrical PCM memories (see e.g. [62]), and up to 34 levels in integrated photonic PCM memories [63]. In such fractionally-crystallised cases, the optical and electrical properties of the resulting mixed phase can be successfully described by different effective medium approximations such as the Bruggeman model, which considers inclusions of crystalline domains in an amorphous matrix or vice versa [58].

The above described properties have made chalcogenide PCMs a suitable platform for the development of nonvolatile memory devices which are nowadays well integrated in commercial technologies. More recently, their potential has been expanded to other fascinating technological fields, such as reconfigurable integrated photonics [30, 64–66] or dynamically tunable metasurfaces and nanoantennas [27, 28, 30–44, 52, 67–72]. However, as mentioned earlier in this section, because the majority of currently available PCMs have their respective optical bandgaps around the 0.7 to 0.8 eV region [53], most of the work carried out up to now in the field of phase-change dynamic metasurfaces is focused in the near-infrared (NIR) and mid-wave-infrared (MWIR), which is where traditional GeSbTe-based phase-change materials possess relatively low optical losses and high optical contrast between their amorphous and crystalline phases [53]. This allows for the design of PCM metasurfaces with sharp, tunable resonances, in turn enabling the development of efficient active meta-devices such as amplitude modulators [42] or low-loss filters [68, 69], and beam steering and lensing based on optical phase modulation [27, 39]. In spite of the relatively strong optical losses present in classic PCMs outside the NIR and MWIR spectral regimes, the use of smart metasurface designs, combined with judicious choice of the PCM alloy used, has allowed researchers to successfully push
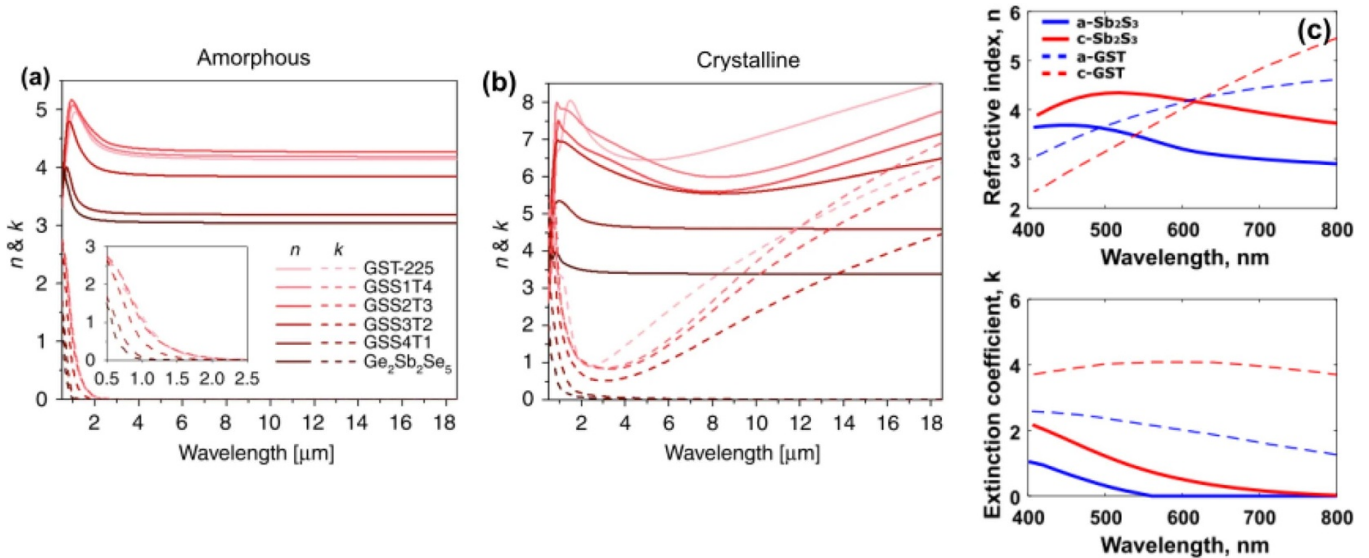
Figure 3. (a), (b) Refractive index n and extinction coefficient k of GSST4 alloys compared to GST225 across the infrared spectrum for (a) amorphous and (b) crystalline states. (c) Refractive index n (top) and extinction coefficient k (bottom) of Sb_2S_3 compared to GST225. (a), (b) Reproduced from [52]. CC BY 4.0. (c) Data extracted from [73].

phase-change metasurface technologies towards more challenging spectral regions, such as the visible and long-wave infrared (LWIR) [36, 37] (where optical losses of GeSbTe and GeTe based compounds become rather high, see figure 2(a)), as well as to minimise the effect of moderate losses present in the NIR and MWIR regimes [27, 42, 52, 68–71].

A good example of such a research trend consists of the use of novel GeSbSeTe alloys, where isoelectronic substitution of Te by Se tends to an increase of the optical bandgap, thus allowing mitigation of optical losses in the infrared [52]. For more clarity, figures 3(a) and (b) show the refractive index of different GeSbSeTe (or GSST) alloys, compared to the classic composition GST225, where a gradually increasing of Se content results in a decrease of the optical losses for both amorphous and crystalline states. Although GSST alloys have shown excellent optical properties across the whole infrared spectrum [52, 72], their optical losses in the visible region are still rather high (and indeed comparable to traditional GeSbTe alloys), and thus still non-ideal for the realisation of photonic meta-devices in the visible. To overcome this problem, Dong *et al* recently proposed the use of Sb_2S_3 [73], a material having significantly lower optical losses in the visible when compared to traditional PCMs, as can be appreciated in figure 3(c). Sb_2S_3 was initially studied as a potential candidate for rewritable optical data storage in the 1990s, but was paradoxically discarded due to low absorption at the visible wavelengths of diode lasers used by that time to write and erase data [73]. While low-loss GeSbSeTe and SbS alloys have emerged very recently as potential candidates to improve the optical performance of phase-change meta-devices, the combination of such PCMs with metasurfaces is still very underexplored, and the majority of the work carried out up to now in the field of dynamically tunable phase-change metasurfaces is based on traditional, well-known GeSbTe and GeTe compositions [26–28, 30–44, 68–70].

In summary, due to their outstanding physical properties, phase-change materials combined with optical metasurfaces offer a technologically important platform for the realisation of a new generation of dynamically tunable, ultra-fast, high endurance and low power consumption photonic meta-devices, capable of operating from the visible right through to the THz regime. In addition, the gradual development of novel (and recovery of old) PCM compositions is opening up a promising possibility towards improving the optical performance of currently reported devices, especially in the more challenging spectral regimes where traditionally employed PCM alloys are affected by relatively high optical losses. In the next sections, we discuss the progress in the field of dynamically tunable phase-change metasurfaces, from the visible to the THz, with special emphasis on the potential applications emerging from such a promising technology, as well as its future perspectives.

3. Tunable phase-change meta-devices in the visible: colour generation

Colour generation employing metasurfaces is a quite well-explored field (see e.g. [74–80]), and is usually achieved by absorbing [76, 77], reflecting [76, 78, 79] or transmitting [74, 80] parts of the visible spectrum by means of plasmonic or dielectric resonant nanoantennas. In such approaches using conventional metasurfaces, however, dynamic control of the colour is not possible; the colours generated are fixed and static, determined by the specific metasurface design used. A far greater range of applications, such as displays, smart-windows and signage, e-readers, etc, would be achievable if dynamic colour control were possible. The scientific community has recently started to explore just such a
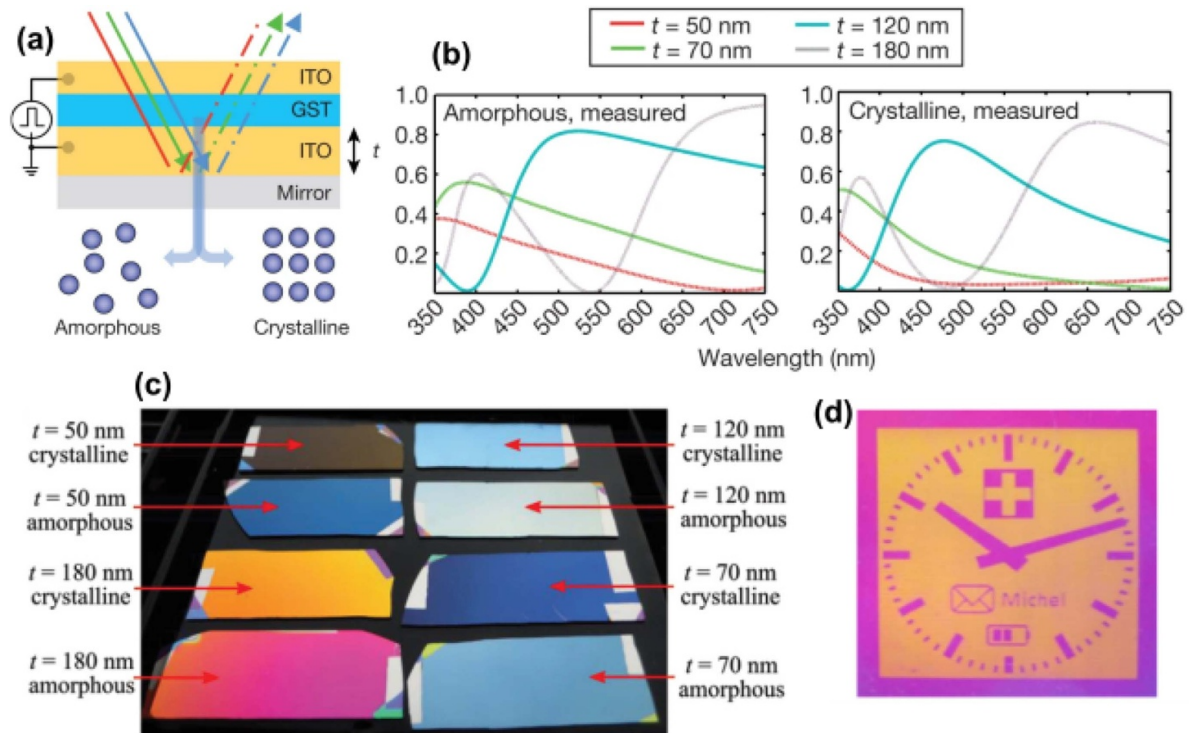
Figure 4. (a) Phase-change material based color displays, consisting of an ITO/GST/ITO layer stack lying on a Pt bottom plane. Structural phase transition of GST can be achieved via applying a voltage between the top and bottom ITO layers. (b) Measured reflectivity spectrum of the devices having different ITO thicknesses and shown in (c), for amorphous (right) and crystalline (left) states. (d) Microscale laser written image. (a)–(c) Reprinted by permission from Springer Nature Customer Service Centre GmbH: Nature [81]. Copyright © 2014, Springer Nature. (d) [87] John Wiley & Sons. © 2017 The Society for Information Display.

possibility, using phase-change metasurfaces among other possibilities [36, 37, 77, 81–86].

The initial experimental demonstration of the capability of PCMs for reconfigurable colour generation was in fact not based on the combination of PCMs with metasurfaces but still relied on resonant effects, this time however via the integration of ultrathin layers of $Ge_2Sb_2Te_5$ in Fabry–Perot (FP) cavities [81]. The approach used is shown in in figure 4(a): an ultrathin (7 nm) $Ge_2Sb_2Te_5$ film is sandwiched between two conductive oxide layers (ITO) to create an electrically addressable optical cavity, the whole structure lying on a reflective metal plane. By employing different cavity designs based on varying the bottom ITO thickness, and switching the PCM layer between its amorphous and crystalline phases, control of the reflected spectrum can be achieved (figure 4(b)), resulting in dramatic changes in colour (figure 4(c)). Dynamic control of the colour generated was achieved in this original work by direct electrical switching of the GST layer, but more recently improved control has been reported using integrated micro-heaters for each individual pixel (see (figure 4(d) and [87]). Alternative PCM compositions, and even combining multiple compositions in the same layer stack, have also been subsequently investigated [73, 83–87].

Since resonant control of reflection/transmission spectra is readily achieved with metasurfaces, it might be expected that phase-change metasurfaces would be well-suited to active colour generation. However, this is in fact quite challenging, due essentially to the relatively large optical losses present in traditional PCMs in the visible part of the spectrum [53, 73]. This in turn results in damping of the metasurface resonances, which fundamentally limits the purity of colours achievable. In fact, the first concepts of dynamically tunable phase-change metasurfaces working in the visible spectrum exploited such strong losses as an advantage to yield reconfigurable broadband absorption having potential applications in solar energy conversion [36, 86], rather than for colour generation. Some of the first experimental demonstrations of phase-change metasurfaces suitable for dynamically tunable colour generation were reported only in the last few years [37, 88]. For example, in [37], Garcia-Cuevas Carrillo *et al* reported the generation of vivid colours employing metal insulator metal (MIM) type metasurfaces combined with the traditional PCM alloy GeTe. Schematics of the device are shown in figure 5(a); the unit cell consists of a dual layer of GeTe and ITO sandwiched between a continuous Al bottom plane and a top Al disk. High purity colours are produced by using the PCM layer as an on/off bottom metallic plane, rather than as a 'dielectric' tunable environment as in typical phase-change material based metadevices [27, 40–44, 67–69, 86]. Therefore, when the GeTe layer is in its amorphous phase, the device is out of resonance (figure 5(b), left). However, GeTe in its crystalline phase behaves optically very much like a metal at visible frequencies (as the real part of its permittivity becomes negative [53, 88]), therefore, crystallisation of the PCM layer results in formation of the characteristic transversal magnetic dipole resonance (figure 5(b), right) supported by MIM metasurfaces [27, 41],
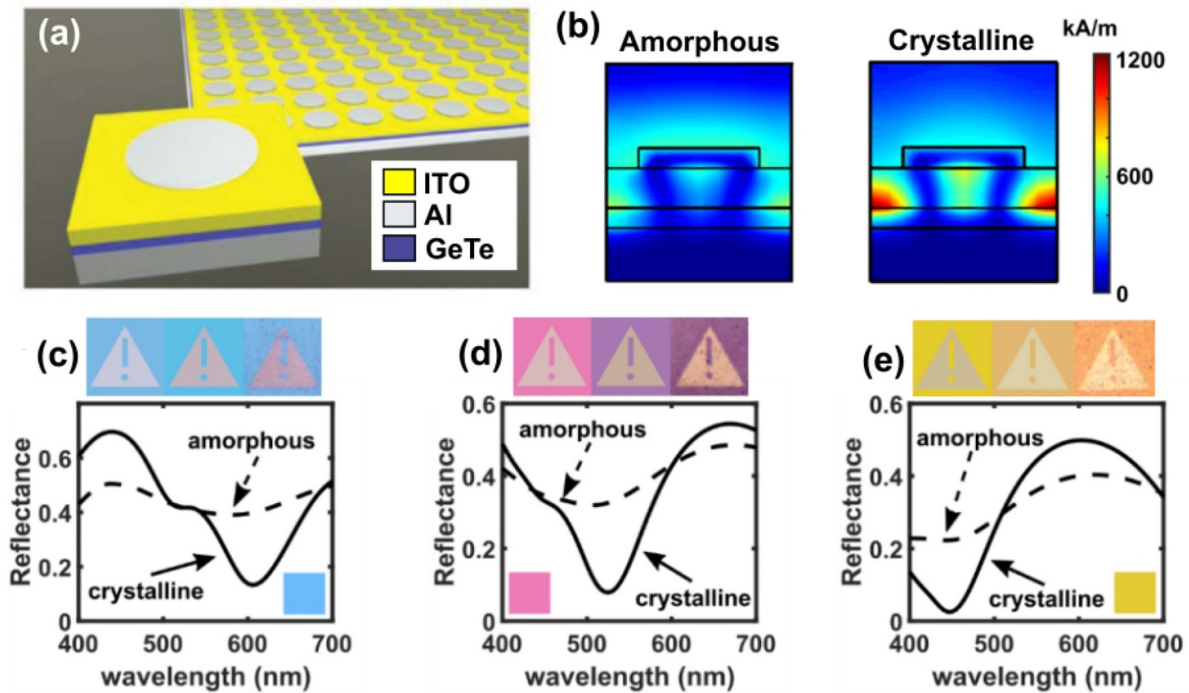
Figure 5. (a) Schematics of the MIM phase-change metasurface absorber. (b) Distribution of of the magnetic field modulus when the device is in its amorphous (off-resonance, left) and crystalline (in resonance, right) phases. (c-1) Reflectance spectrum for amorphous (dashed) and crystalline (solid) of the cyan (c) magenta (d) and yellow (e) pixels. Images at the top of the plots represent the theoretical as designed, theoretical as-gabricated and experimentally obtained colours from left to right. Reproduced from [37]. CC BY 4.0.

with energy being strongly coupled to, and thus absorbed by, the array of unit cells. Taking advantage of resonant behavior, a set of dynamically tunable cyan, magenta and yellow pixels were designed (via variation of the unit cell period, Al disk radius and ITO thickness), fabricated and experimentally demonstrated, as shown in figures 5(c)–(e). As can be seen, when the GeTe layer is crystalline, the resonant absorber selectively absorbs the red, green and blue spectral bands of the visible spectrum, resulting in cyan (figure 5(c)), magenta (figure 5(d)) and yellow (figure 5(e)) colours in reflection. Switching the GeTe to the amorphous phase results in a flat reflectance spectrum (the resonance is 'turned off'), with a subsequent white-like visual appearance. By such means, the authors suggested the use of such structures as a way to obtain a full colour palette using standard subtractive colour techniques.

4. Tunable phase-change meta-devices in the near-infrared

The near infrared (NIR) is a technologically important spectral band, with many key applications in areas such as optical communications, biosensing and night vision (non-thermal) imaging. As a result, over the last decade an enormous research effort has been put into the development of conventional metasurfaces operating in this regime, including superabsorbers [19], filters [89], lenses [90], beam steerers [91], or holograms [92], which could potentially replace bulky optical components of current NIR optical systems. More recently,

research has been re-focused towards adding tunability and reconfigurability to such devices, employing a variety of different techniques (see e.g. [9, 27, 31, 41, 42, 71, 92–94]). Indeed, the use of phase-change metasurfaces has played an important role in this respect [27, 31, 41, 42, 44, 70, 93–98], perhaps due to the excellent optical contrast with low optical losses that traditional PCM compositions present in the NIR spectral band [53]. As a result, a number of exciting dynamically tunable NIR PCM meta-devices for amplitude and phase control has emerged, including active filters [43], band switches [35, 96], beam steerers [27, 95], and integrated and free-space super absorbers and modulators [41, 42, 93, 97, 98].

4.1. Phase-change meta-devices for amplitude control in the NIR

4.1.1. Phase-change metasurfaces for free-space applications. Selective, low power consumption, ultrafast and dynamically tunable control of light amplitude in the NIR (particularly in the O and C telecommunication bands) could find many important technological applications in the field of optical signal processing. In this context, the ability of metasurfaces to control the amplitude of light at will, combined with PCM alloys whose refractive indices can be reversibly and abruptly controlled in a non-volatile way, could therefore result in a new generation of compact spectral switches, absorbers and modulators employed in optical telecommunications and related fields.
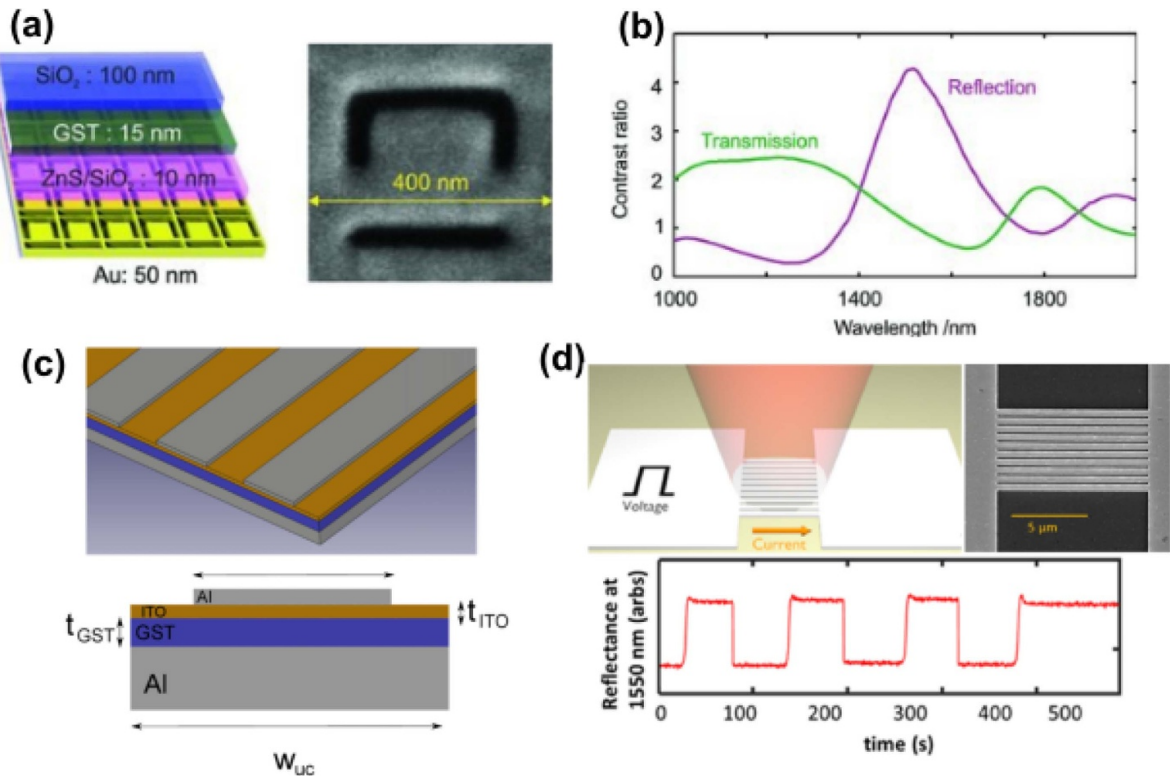
Figure 6. (a) Schematics of the NIR phase-change meta-switch (left) and scanning electron microscope image of one of the fabricated devices (right). (b) Transmission (green) and reflection (purple) contrast ratio across the near infrared obtained when changing the device shown in (a) between amorphous and crystalline phases. (c) Schematics of the MIM based phase-change metasurface for reconfigurable absorption and modulation in the NIR. (d) Experimentally obtained reflectance spectrum after various crystallisation and re-amorphisation laser scans (left) and optical images of the device after each scan (right). (a), (b) [35] John Wiley & Sons. Copyright © 2013 WILEY-VCH Verlag GmbH & Co. KGaA, Weinheim. (c), (d) Reproduced from [93]. CC BY 4.0.

Some of the first phase-change meta-devices for active amplitude control operating in the NIR appeared around a decade ago now [35, 96, 97]. Such devices were based on arrays of plasmonic meta-atoms mostly combined with the archetypal PCM alloy $Ge_2Sb_2Te_5$. For instance, in 2013 Gholipour *et al* reported one of the first experimental demonstrations of phase-change meta-devices for spectral switching and filtering in the NIR [35]. Here, a gold/insulator plasmonic metasurface consisting of Babinet inverted split ring resonators was combined with a multilayer stack including GST as a tunable dielectric environment, as depicted in figure 6(a). The design was optimised to support narrowband Fano resonances, resulting in a sharp transmission peak at a specific NIR band when the PCM is amorphous. After crystallisation of the GST layer, the resonant transmission peak is shifted towards larger wavelengths due to an increase of GST refractive index, thus providing for signal modulation in both transmission and reflection simultaneously, as depicted in figure 6(b). Switching of the GST layer between states was achieved by ex-situ laser excitation.

More recently, further developments of PCM-based metasurfaces for various applications in the NIR have been made, including, for instance, metal-insulator-metal configurations where the insulator layer is substituted by a PCM which acts as a tunable environment [27, 41, 93, 97, 98]. For example, figures 6(c)–(d) show results from recent work by Garcia-Cuevas Carrillo *et al* [41, 93], where a continuous GST layer is sandwiched between an Al bottom plane and a patterned 1D Al antenna (figure 6(c)). By appropriate design of the geometrical parameters of the basic unit cell and by switching the GST layer between phases, the authors showed super absorption/modulation of the C-band (1550 nm) with on-demand pre-designed quality factors. Both ex-situ optical switching (via laser scans) and *in-situ* electrical switching (by using the top metasurface as a series of electrical micro-heaters) of the PCM layer were successfully demonstrated (see figure 6(d)).

In all the above meta-device examples, phase-change materials were combined with plasmonic metasurfaces to deliver tunability. However, such approaches invariably suffer from plasmonic (ohmic) losses, which in turn limit the efficiencies that can be achieved, especially in transmission. To overcome such limitations, de Galarreta *et al* showed more recently the possibility of creating low loss, high efficiency optical meta-filters and modulators employing an all-dielectric approach in which the metasurface consists of an array of hybrid silicon/GST nanocylinders [68, 69]. The basic unit cell (depicted in figure 7(a)) consists of a low aspect ratio, high index silicon nanocylinder with an embedded ultrathin GST layer (15 nm). Exploiting the advantage of a near matching between the refractive indices of silicon and amorphous GST, the dimensions of the cylinders were optimised to support spectrally separated electric and magnetic Mie reflectivity resonances falling in the O and C telecommunication bands,
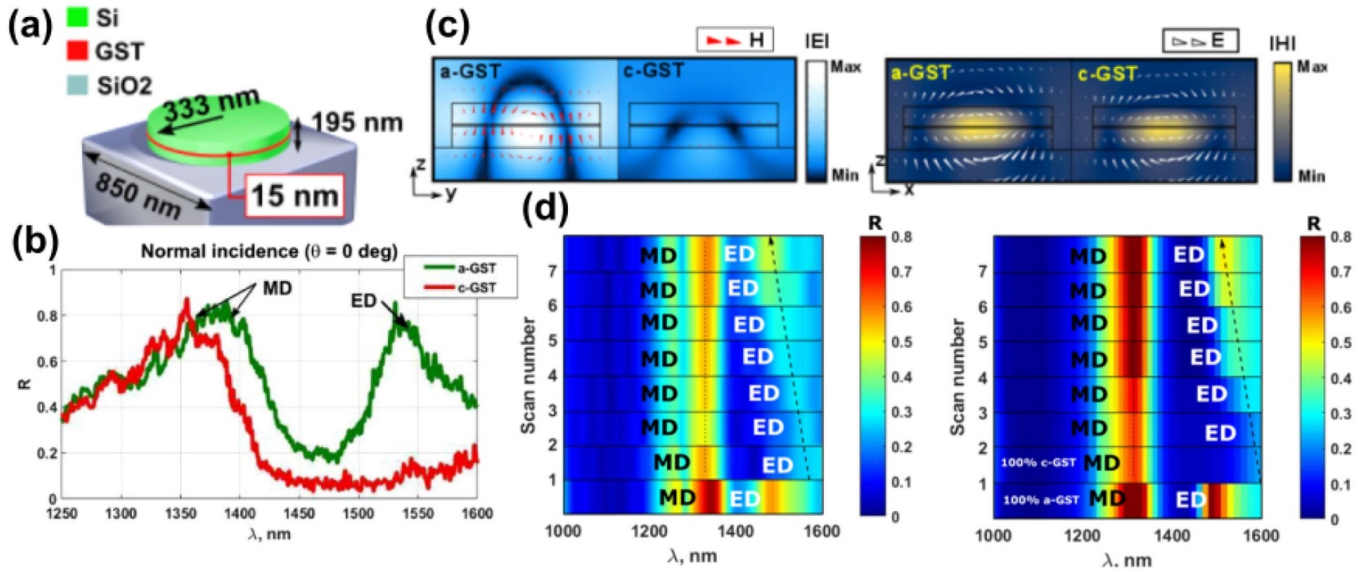
Figure 7. (a) Schematics and dimensions of the hybrid silicon/PCM metasurface consisting of arrays of silicon/GST nanodisks on a SiO$_2$ substrate. (b) Measured reflectance spectrum for showing the presence of two reflectance peaks in the O and C bands, corresponding to the MD and ED resonances when the GST layer is amorphous (green), and only one resonant peak corresponding to the MD after crystallisation. Inset shows a scanning electron microscope image of one of the fabricated devices. (c) Electromagnetic field distribution for amorphous and crystalline states of the ED (left) and MD (right), showing disturbance and conservation of the ED and MD respectively after GST crystallisation. (d) Experimental evolution of the reflectance spectrum (colourbar) after several laser scans showing up to nine levels of tunability (left), and compared to simulations (right). Reproduced from [69]. CC BY 4.0.

thus creating a dual-band filtering behaviour. As shown in the measured reflectance spectrum (in figure 7(b)), this results in two resonant reflectance peaks at the desired (O and C band) wavelengths when the GST is in its amorphous phase. After crystallisation of the layer, however, the electric dipole (ED) resonance is cancelled, thus C band is now transmitted (instead of being reflected) while the O band corresponding to the magnetic dipole (MD) remains nearly unaffected. This was achieved by strategic placement of the GST layer in the antinodes of the electric field of the ED mode, which disturbs the resonant mode after the change of the complex refractive index upon crystallisation (figure 7(c), left), but conserves the MD intact due to small interactions of the GST layer with the electric fields (figure 7(c), right). Reflection efficiencies as high as 80% were achieved, much higher than those typically obtained with plasmonic approaches. Absolute contrasts in the C band of 70% in reflection ($\Delta R = R_{am} - R_{cr}$) and 65% in transmission ($\Delta T = T_{am} - T_{cr}$) were achieved using only 15 nm of GST, i.e. the highest optical contrast-to-PCM volume ratio achieved so far in phase-change metasurfaces. This ratio is an important factor to take into account in phase-change metasurface designs, as the large volumes of PCM sometimes required for an optimum optical contrast in PCM-based metasurfaces might not be easy (even impossible) to switch reversibly (i.e. re-amorphised). This is due to self-thermal insulation of PCMs which inherently possess relatively low thermal conductivities [92]. As a result, large PCM volumes take longer to cooldown after melting, so that metasurface/device designs with thick PCM layers might not be successfully re-amorphised due to the high cooling rates required for the latter (as depicted in figure 2(b)). The limit on

practicable PCM volume/thickness in any particular design depends on the thermal properties (thermal conductivity, specific heat, and density) of the PCM itself, as well as those of surrounding layers/materials. Indeed, due to the small GST volume employed in their design, de Galarreta *et al* were able to demonstrate, for the first time, multilevel and fully reversible switching in the C band (via crystallisation and subsequent step-by-step partial re-amorphisation employing femtosecond laser excitation at a central wavelength of 1050 nm)—see figure 7(d). The combination of ultrathin layers of PCM within the body of high index resonators to form metal-free, all-dielectric tunable PCM metasurfaces reported by de Galarreta *et al* provides a most attractive route towards the realisation of high optical performance, non-volatile, fully reversible and multilevel tunable meta-devices. However, the incorporation of metal layers into PCM metasurface designs, while invariably introducing plasmonic losses, does bring with it the advantage of potentially using such metal layers as embedded micro-heaters for *in-situ* switching of the PCM layer (in a similar way to demonstrated in figure 6(d)). To address this issue, a novel PCM metasurface design offering potentially the 'best-of-both-worlds' was recently proposed, namely a hybrid all-dielectric/plasmonic approach comprising arrays of silicon-/GST meta-atoms atop a metallic plane [42, 99]. The approach is summarised in figure 8 [42], where it can be seen that the basic structure (figure 8(a)) consists of arrays of high index cubic silicon resonators with an embedded thin GST layer. Contrary to the all-dielectric approach, the whole structure here lies on a metallic plane (here Al, but Au has also been used successfully [99]) which, as previously mentioned, could (suitably patterned) be used as an *in-situ* resistive heater
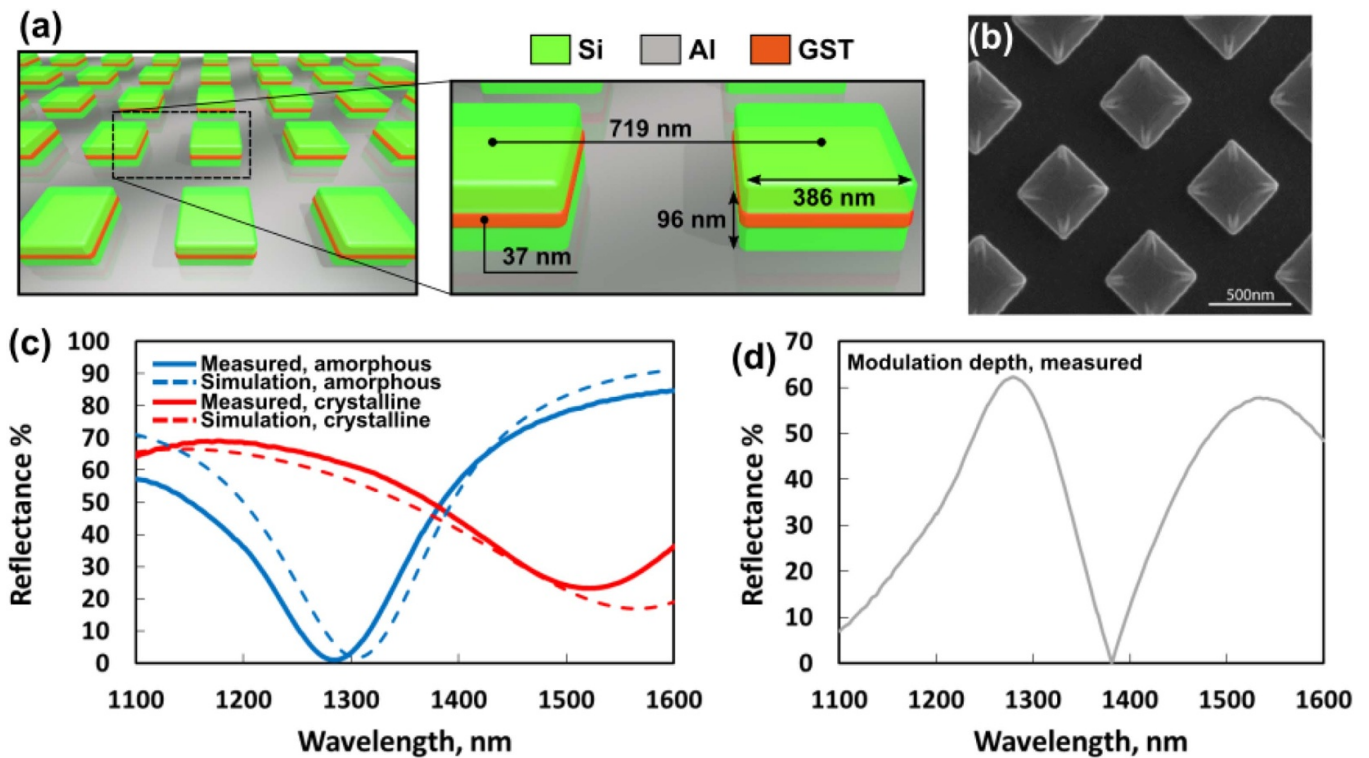
Figure 8. (a) Schematics and dimensions phase-change metasurface NIR dual band modulator. (b) SEM image of one of the fabricated structures. (c) Measured (solid) reflectance spectrum compared to simulations (dashed) for both amorphous and crystalline phases of GST. (d) Measured modulation depth showing aound 60% of modulation at both the O and C bands. Reproduced from [42]. CC BY 4.0.

to induce phase transitions of the PCM. The geometrical parameters were optimised to support transverse magnetic resonances to selectively absorb the O and C telecom bands when the PCM is switched from amorphous and crystalline phases, thus to operate as a simultaenous modulator at 1310 and 1550 nm wavelengths respectively. An SEM image of the realised structure can be seen in figure 8(b), while figure 8(c) shows the experimental and simulated reflectance spectra, which are in excellent agreement and demonstrate absolute modulation depths of ~60% for both the O and C bands (figure 8(d)), employing only 37 nm of GST as an active medium.

4.1.2. Phase-change meta-devices for integrated photonics.
In addition to the use of phase-change materials for the realisation of free-space reconfigurable photonic meta-devices with amplitude control capabilities in the NIR, they have been also successfully employed in integrated photonic devices to provide amplitude modulation, switches, couplers. etc [100–107], and, interestingly, to provide entirely new types of all-optical non-volatile memory and all-optical arithmetic and neuromorphic processing [64, 66, 101–104]. In such devices, light guided through an integrated waveguide (typically made of SiNx or Si [100–105]) can be used to selectively change the structural phase of microscale PCM cells located on top of the waveguide. Such structural phase transformations result in a change in the amplitude of a read pulse sent down the waveguide, as a direct consequence of changes of the refractive indices and extinction coefficient of the PCM cell.

This innovative concept, developed by Bhaskaran, Pernice, Wright and co-workers [63, 64, 66, 101–104] is summarised in figure 9, where in this example the device (figures 9(a) and (b)) consists of a Si$_3$N$_4$ waveguide with a 10 nm thick GST cell (and covered with an ITO layer to avoid oxidation). The dimensions of the waveguide were optimised to support the fundamental TE mode at the C band, as can be appreciated by the electric field distribution shown in figure 9(c), The authors were able to write and read 8 amplitude levels (via partial crystallisation of the PCM) in a single cell (figure 9(d)), and more recent work by the same team has extended this to 32 levels [63] and integrated multiple cells to provide small-scale optical chips with 512 bit capacity [102]. As with all memory and device developments, however, for improved performance there is an ever present need to try to both reduce the energy required for switching, and to increase the switching speed. In this context plasmonic nanoantennas can be used to good effect. For instance, Gemo *et al* [65] recently reported the use of plasmonic nanoantennas to enhance light matter interaction between the propagating waveguide mode and the PCM cell The basic structure is summarised in figure 10(a). The usual GST cell arrangement is here substituted by an Ag dimer plasmonic antenna to provide an increase light confinement within its gap, which is filled by GST. This leads to a dramatic increase in the interaction between the propagating mode and the GST itself, as shown in figure 10(b) where the electric field enhancement factor, *EF,* produced by the plasmonic antenna is plotted as a function of the antenna's geometrical parameters. *EF* values as high as 600 are achieved
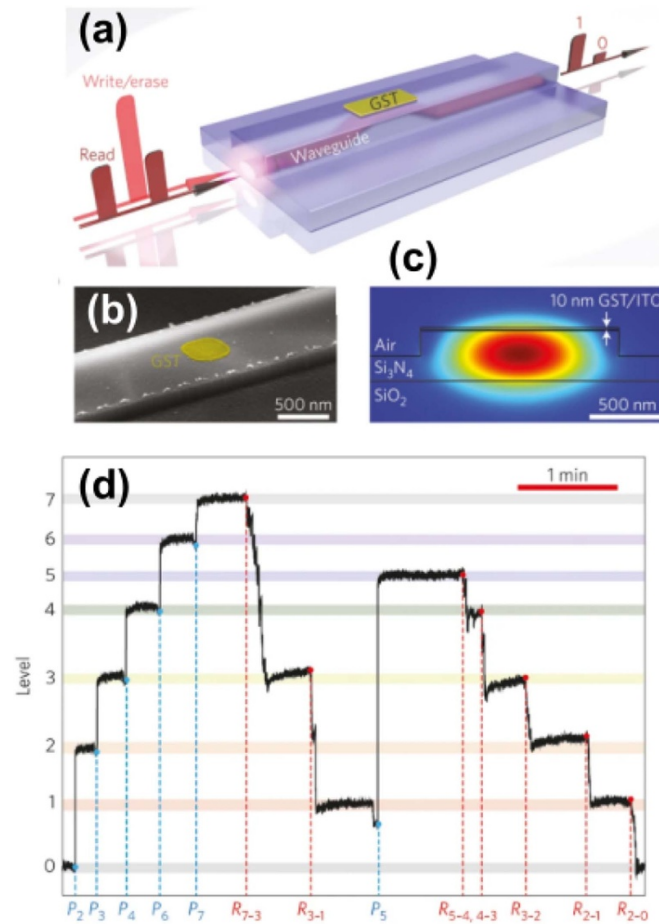
Figure 9. (a) Schematics showing the working principle of PCM-based reconfigurable integrated photonics. NIR light pulses with different powers and durations can be used to change the structural phase of the PCM top layer, resulting in an output signal modulation. (b) Scanning electron microscope image of one of the fabricated devices, with the GST patch highlighted in false colour. (c) Cross section of the waveguide showing the electric field distribution of the TE mode, when the GST layer is amorphous. (d) Experimentally-obtained readout levels (a total of eight) achieavable employing different pulse lengths/energies. Reprinted by permission from Springer Nature Customer Service Centre GmbH: Nature Photonics [64]. Copyright © 2015, Springer Nature.

for very small gap widths (e.g. for the case of a dimer antenna of 70 nm radius with a gap width of 10 nm). As a result of such large electric field into the integrated photonic memory type devices of figures 9 and 10 also brings with it the potential advantage of enabling direct electrical switching of the PCM cell. This can be achieved by using the nanoantennas also as electrodes, across which a voltage can be applied to switch the cell. In this way 'mixed-mode' operation of the device can be obtained, i.e. the device can be written electrically and read optically, written optically and read electrically, or written and read entirely in a single domain. Indeed, Farmakidis *et al* [105] recently experimentally demonstrated just such a device, as shown in figure 10(c).

4.2. Phase-change metasurfaces for wavefront engineering in the NIR

In the developments reported above, we have so far been primarily concerned with controlling the amplitude of light interacting with a metasurface. However, metasurface control of the optical phase of wavefronts would open up a

new route towards the next generation of lightweight, high efficiency, reconfigurable optical components such as flat lenses, axicons or beam steerers. Optical metasurfaces for local phase control, or the so-called 'phase-gradient metasurfaces', emerged nearly a decade ago [4], and share the essence of the well-established antenna technology used in the radio- and microwave regimes, where the phase of an input beam is locally controlled by means of resonant elements (antennas) to generate a particular output wavefront. These devices can be therefore employed to mimic the wavefront engineering capabilities of conventional bulky optics, but with discrete optical phase control capabilities relying on localised optical phase jumps coming from subwavelength resonant elements (instead of propagation effects as in bulky optics). In addition, extending the capabilities of phase-gradient metasurfaces towards dynamic wavefront engineering would open up a new route to a variety of exciting applications involving active lensing, or beam steering with no moving parts. This includes, for instance, light detection and ranging (LIDAR) systems for autonomous vehicles and robotics, and free-space optical signal coupling. Very recently, the combination of chalcogenide
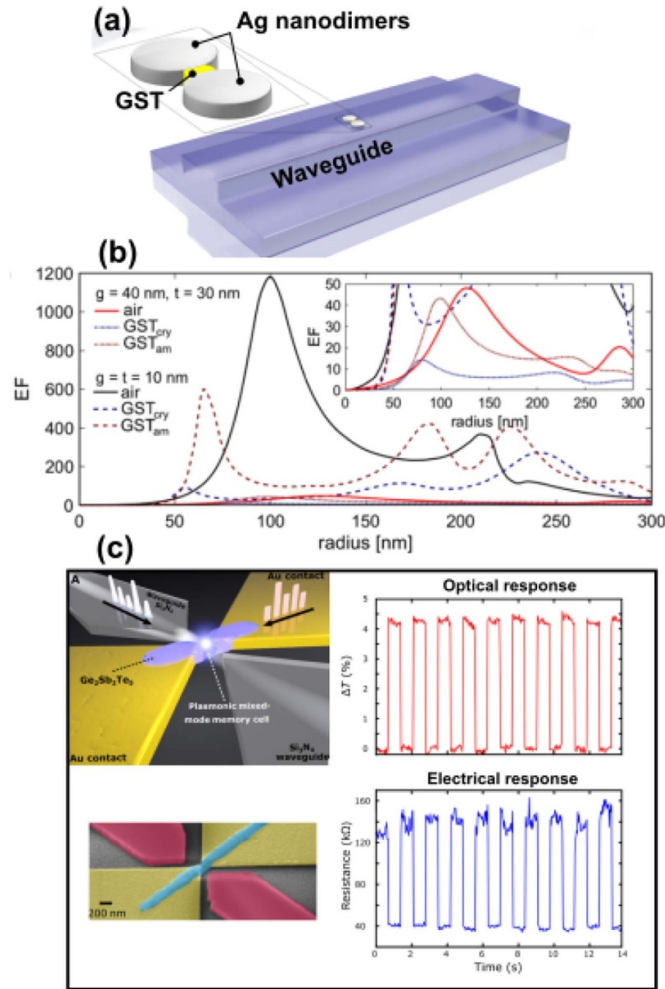
Figure 10. (a) Schematics of the plasmonically enhanced all-optical integrated phase-change memory. The usual PCM (here GST) cell arrangement on top of the waveguide (left) is replaced with a plasmonic dimer nanoantenna with GST deposited into the gap between the two parts of the dimer structure. (b) Graphs showing the effect of the Ag dimer's geometrical parameters (i.e. radii and gap) on the electric field enhancement factor EF. (c) Plasmonic mixed-mode phase-change integrated photonic devices. (a), (b) Reproduced from [65]. CC BY 4.0. (c) Reproduced from [105]. CC BY 4.0.

phase-change materials with phase-gradient metasurfaces has emerged as a way to achieve reconfigurable optical-phase manipulation in the NIR [27, 95, 99, 108, 109]. Most of the work carried out to date relies on simulations to showcase exciting novel device concepts for either binary or multiple angle beam steering [95, 99, 108, 109]. However, the first successful experimental demonstration of optical phase control in the NIR employing PCMs was recently published by de Galarreta *et al* [27]. In this work, the use of plasmonic metasurfaces combined with thin GST films for dynamically tunable binary beam steering in the C-band (from $\lambda = 1510$ nm to $\lambda = 1580$ nm) was proposed and experimentally validated. The schematics of the proposed PCM metadevice are shown in figure 11(a). It consists of a SiO_2, ITO, GST and ITO multilayer stack, sandwiched between a continuous Al bottom plane and a top array of periodically arranged 1D plasmonic Al antennas (strips). By varying the top Al antenna widths, thus changing the unit cell resonant frequency, a total optical phase span of 300° can be achieved in reflection when the GST layer is amorphous. A linear optical phase gradient can be therefore

imposed along the surface of the device (x-direction in figure 11(a)) at the design wavelength of $\lambda = 1550$ nm, via formation of a super cell containing four antennas having a shown in figure 11(b), right, in a constructive interference at a pre-designed angle (here specifically 33.6°) of anomalous reflection dictated by the generalised Snells' law [4]. Crystallisation of the GST layer results in a red-shift and damping of the antenna resonant frequency, limiting the optical phase-response to negligibly small variations with the Al antenna width. In such a way, the selected antenna widths result in a near invariant spatial optical phase response with the GST layer crystalline, so yielding conventional specular reflection (figure 11(b), left). The devices were successfully fabricated, see figure 11(c) and optical characterisation revealed the desired steering angle of ∼33° was achieved when the GST layer was amorphous, and specular reflection achieved when it was crystalline, see figure 11(d). Reflection efficiences as high as ∼35% were achieved, rather high for plasmonic type devices. Reversibility (i.e. crystallisation and re-amorphisation) of the device was successfully realised employing laser excitation.
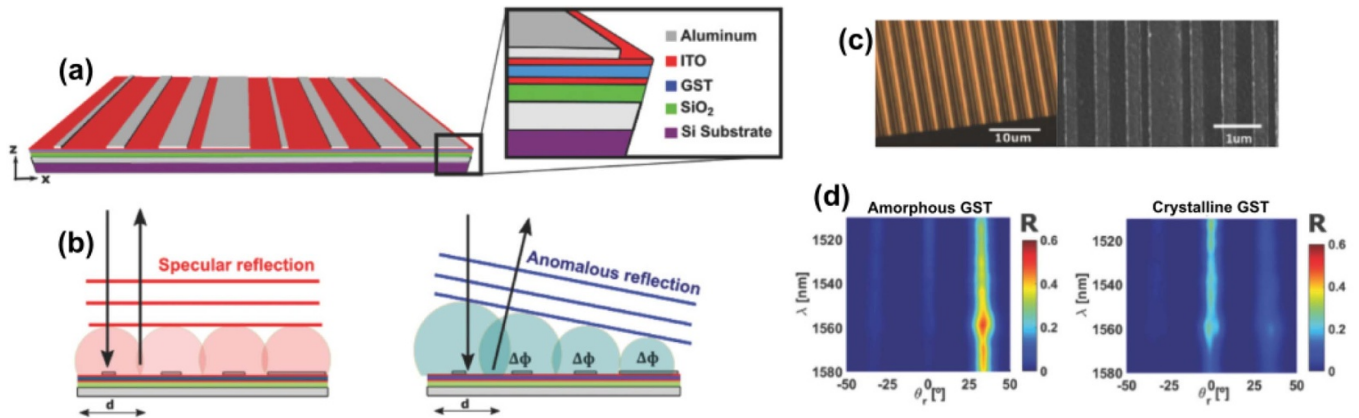
Figure 11. (a) Structure and materials employed in the phase-change plasmonic metasurface for beam steering in the NIR. (b) Huygens principle showing the wavefront reconstruction under normal incidence when the GST layer is amorphous (left) and crystalline (right). (c) Optical microscope and SEM images of one of the fabricated structures. (d) Measured angular reflectance revealing anomalous reflection when the GST layer is amorphous (left) and conventional specular reflection after crystallisation (right). [27] John Wiley & Sons. © 2018 WILEY-VCH Verlag GmbH & Co. KGaA, Weinheim.

Obtaining higher efficiencies in plasmonic-based PCM metasurfaces for phase-only control is difficult, due to inherent plasmonic and dielectric losses present in metals and PCMs respectively, which in turn leads to a dampening of the resonances and significantly reduces the phase coverage and efficiency attainable. However, the recent development of low loss PCM compositions, such as GeSbSeTe [52], together with the use of alternative non-plasmonic metasurface configurations (such as PCM-based all-dielectric [68, 69] or hybrid dielectric/plasmonic resonator arrays [42, 99]) could provide a route to significant improvements in efficiency. In fact, such considerations are being currently explored in the mid-wave infrared [71, 72], as we will see in the next sections.

5. Tunable phase-change meta-devices in the mid and long-wave infrared

Mid-wave (MWIR) and long-wave infrared (LWIR) spectra (sometimes denoted as thermal IR) can be used for the detection of temperatures ranging from that of the human body to 700 °C. In addition, such regimes can excite molecular rotational and vibrational modes. This makes MWIR and LWIR radiation an attractive spectral regime for applications ranging from thermal imaging for security, defence and medicine, to spectroscopic biosensing [110]. Research interest in the development of compact metasurfaces operating in such spectral bands has been therefore growing fast over the past decade, resulting in the development of many suitable devices including flat lenses, polarizers, beam steerers spectral filters and much more [4, 111–116]. More recently, chalcogenide phase-change materials have played an important role in adding tunability to these devices, particularly for amplitude control in the MWIR where the refractive indices of some of the traditional GeSbTe compositions show high optical contrast and moderate optical losses [53, 67]. Furthermore, the emergence of novel low loss compositions based on GeSbSeTe [52, 72], as well as the combination of smart and practicable metasurface

designs with GeSbTe alloys [38, 68, 69, 71, 72, 113, 116], has resulted in the first demonstrations of devices for active wavefront engineering based on phase-only control in the MWIR, as we will see below.

5.1. Phase-change meta-devices for amplitude control in the MWIR and LWIR

In analogy to amplitude metasurface modulators or frequency selective filters working in the visible and NIR spectral regions, devices for amplitude control in the MWIR and LWIR are based on a relevant portion of the spectrum being selectively absorbed, reflected or transmitted., In the MWIR and LWIR regimes selective control of light amplitude is highly desirable for applications such as multispectral and thermal imaging, biosensing [43, 117, 118] or thermal emission [119]. A recent example of using PCM-based metasurfaces for multispectral imaging in the MWIR and LWIR was reported by Trimby et al, where tunable frequency selective metasurfaces based on the extraordinary transmission (EOT) effect combined with PCMs were developed [43] (based on previous work from Rudé et al in the NIR [120]). Their approach is summarised in figure 12. A schematic of the device is shown in figure 12(a), where it can be seen that the device consists of an array of sub-wavelength circular holes in a thin gold film, combined with a GST layer (capped with Si_3N_4 to avoid oxidation). Devices operating in the LWIR were successfully fabricated (figure 12(b)) and tested (figure 12(c)), and designs for MWIR were also developed (figure 12(d)). As can be seen, the devices are capable of selectively filtering a specific IR spectral band when the GST is amorphous, with the centre frequency of the transmitted band shifting to longer wavelengths after crystallisation. Multispectral imaging capabilities could be therefore achieved via changing the PCM layer gradually between purely amorphous and purely crystalline phases (resulting in a gradual shift in the transmission peak position) while simultaneously capturing multiple images. Here again, a damping (broadening) of the resonances due to the increase in
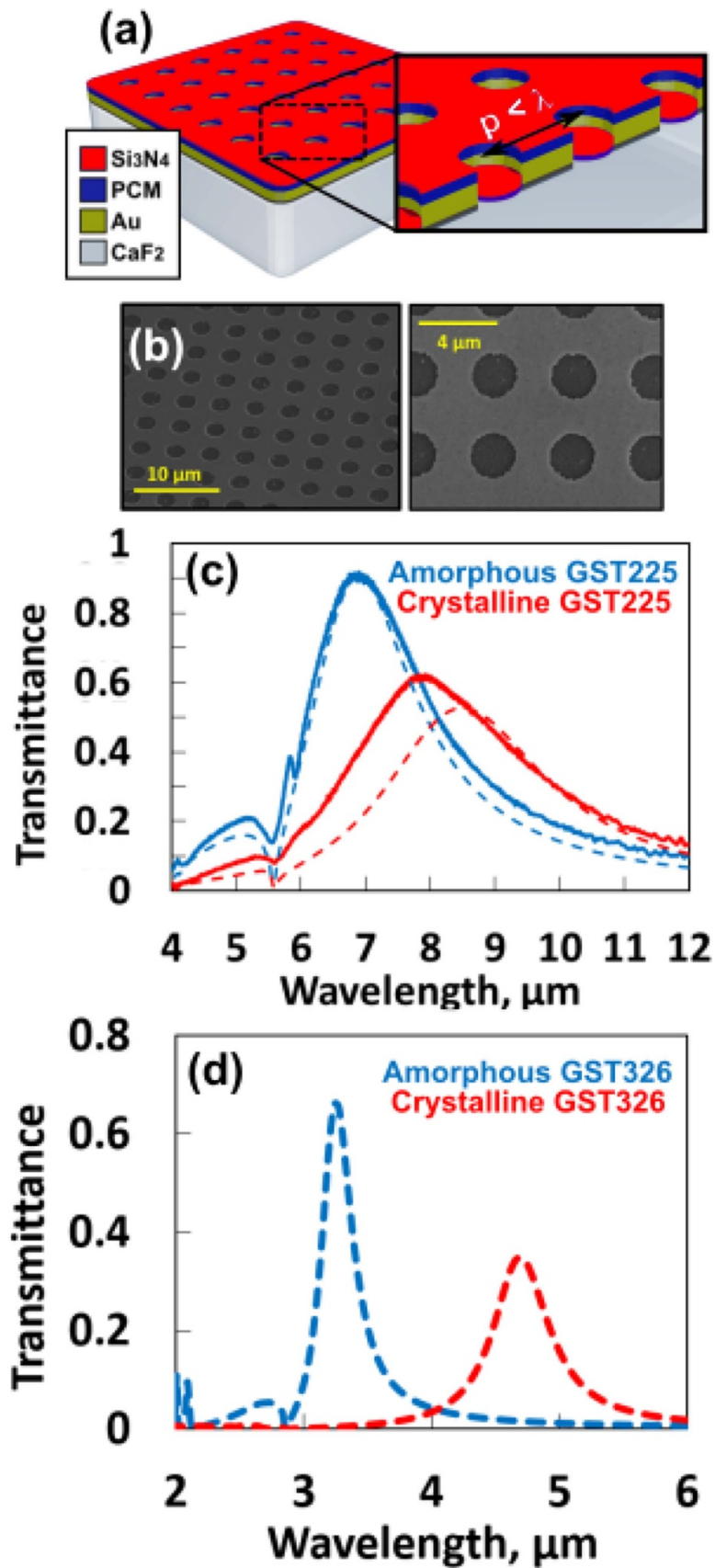
Figure 12. (a) General schematics of the EOT-like phase-change metasurface, whose dimensions can be optimised to operate either in the MWIR or LWIR spectral regimes (b) SEM images of one of the fabricated devices. (c) Experimental transmittance spectrum (solid) for amorphous and crystalline $Ge_2Sb_2Te_5$ compared to simulations (dashed) of the fabricated phase-change band-pass filter. (d) Simulated spectra for a device optimsed to work in the MWIR. Reproduced with permission from [43].
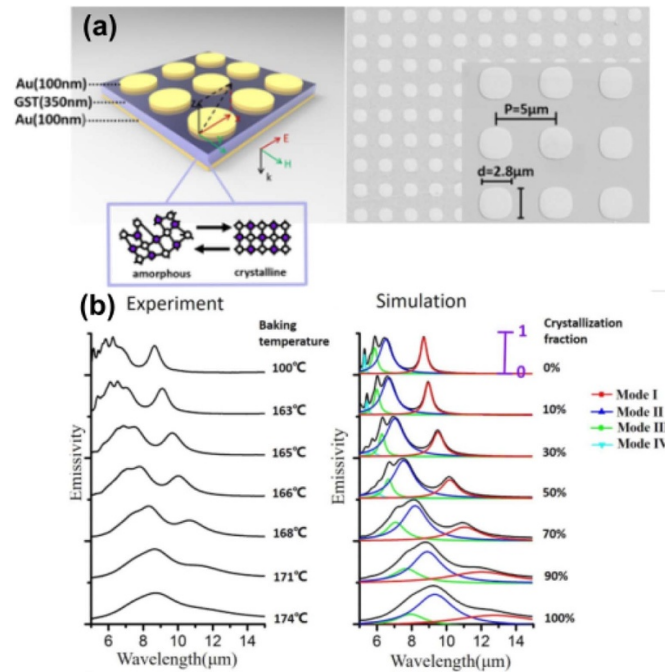
Figure 13. (a) Schematics of the phase-change MIM thermal emitter and SEM image of the fabricated device. (b) Experimental (left) and theoretical (right) emissivity evolution as a function of the GST fraction of crystallisation, associated with different experimental annealing temperatures. [119] John Wiley & Sons. © 2017 WILEY-VCH Verlag GmbH & Co. KGaA, Weinheim.
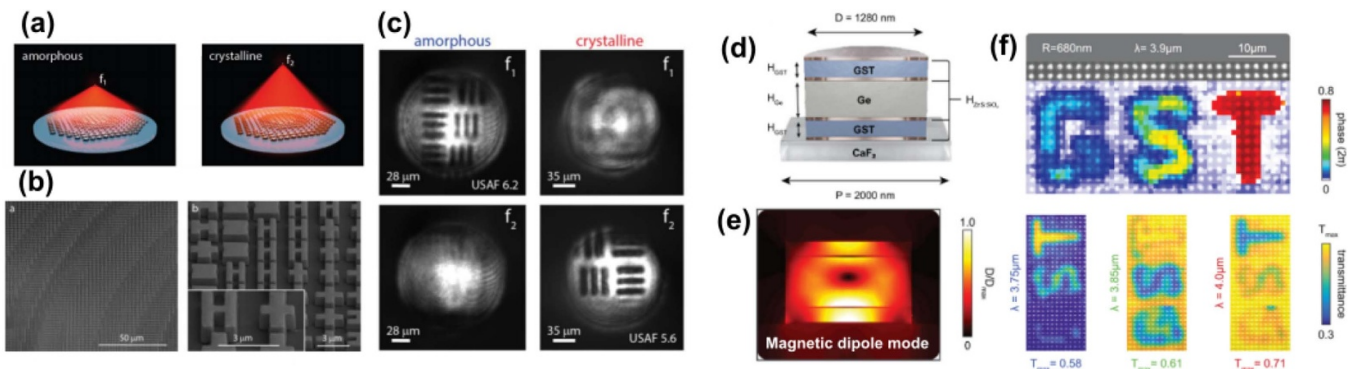

Figure 14. (a), (b) Working principle of the GSST2241 based varifocal metalens (left) and required hyperbolic phase profile (right) for (a) amorphous, and (b) crystalline GSST2241. (c) Images of USAF tests obtained employing the varifocal PCM metalens, and revealing resolution limits of 7 and 9 μm for amorphous (left) and crystalline (right) states respectively. (d) Schematics of the unit cell and dimensions of the proposed phase shifters, showing a Ge cylinder with embedded GST326 layers with incorporated ZnS:SiO$_2$ buffer layers. (e) Simulated displacement electric field profiles at the magnetic dipole resonance, where GST325 layers coincide with the displacement field maxima. (f) Laser-induced arbitrary phase distribution employing cylinders with different degrees of crystallisation, with the letters 'G', 'S' and 'T' encoded. (a)–(c) Reproduced with permission from [72]. (d)–(f) [71] John Wiley & Sons. © 2020 WILEY-VCH Verlag GmbH & Co. KGaA, Weinheim.

extinction coefficient upon crystallisation can be appreciated. Again, this might be ameliorated by use of lower-loss PCM compositions, such as GSST [52].

Another recent example of the technological potential of phase-change metasurfaces operating in the MWIR and LWIR was demonstrated by Qu *et al* [119], with the creation of tunable thermal emitters. The proposed device is shown in figure 13(a), and consists of a GST layer sandwiched between an Au bottom plane, and a top patterned plasmonic structure in the form of Au disks (forming a MIM metasurface). As can be seen from the measured and simulated emissivity spectra (figure 12(b)), gradual thermal crystallization of the GST resulted

in emissivity being shifted towards longer wavelengths, with the higher order, high Q-factor modes being suppressed due to the characteristic optical lossess present in crystalline GST.

5.2. Phase-change metasurfaces for wavefront engineering in the MWIR

Thanks to the evolution of phase-change metasurface architectures towards more practicable designs [68, 69, 71, 116, 119, 121, 122], combined with the emergence of novel low-loss PCM compositions [72, 116], initial devices for phase-only dynamic wavefront engineering in the MWIR have recently
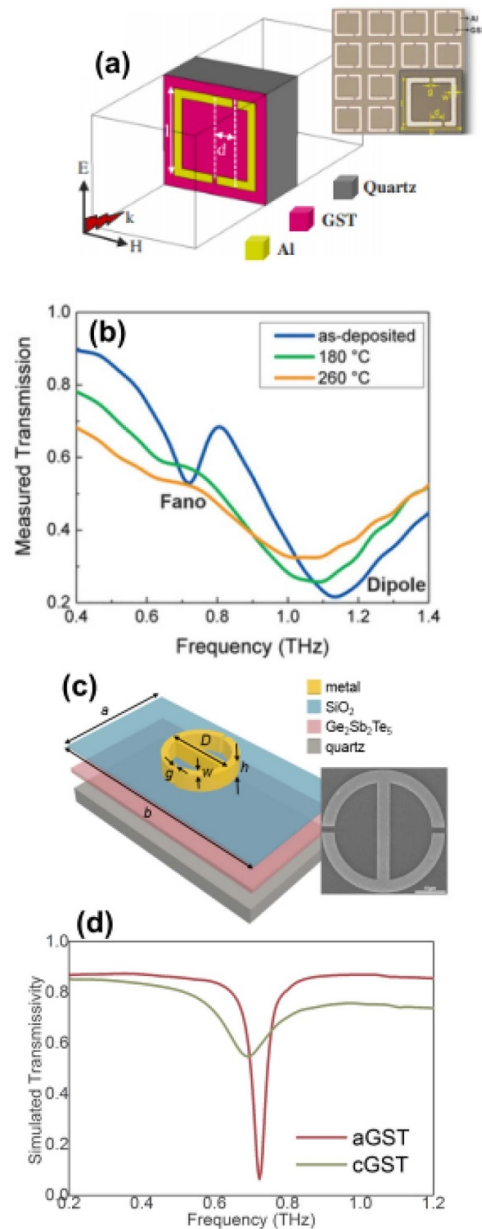
Figure 15. Schematics of the THz phase-change metasurface based amplitude modulator, consisting of Al asymmetric split ring resonators lying on thin GST films. Inset shows an SEM image of the fabricated device. (b) Measured transmission spectrum for as-deposited, and annealed GST at 180 and 250 °C. (c) Transmission THz phase-change amplitude modulator employing Au symmetric split ring resonators on GST thin films. (d) Simulatied transmission spectrum for amorphous and crystalline phases of GST, showing a narrowband modulation between phases of 55% at 0.77 THz. (a), (b) [131] John Wiley & Sons. © 2019 WILEY-VCH Verlag GmbH & Co. KGaA, Weinheim. (c), (d) Reproduced with permission from [132].

been reported in the form of reconfigurable flat lenses [72, 121] and reconfigurable optical phase-shifters [71]. For instance, Shalaginov *et al* recently reported the use of directly structured $Ge_2Sb_2Se_4Te_1$ (GSST2241) as low-loss, high index tunable dielectric resonators to yield varifocal lenses operating at a wavelength of 5.2 μm [72]. The device working principle is summarised in figure 14(a), where periodically arranged GSST2241 amorphous dielectric resonators having different shapes and sizes are arranged to impose an hyperbolic phase profile on incident light, resulting in light being focused at a pre-designed focal length $f_1 = 1.5$ mm. Crystallisation of

the GSST resonators results in a change in the hyperbolic phase profile, with a subsequent change in the focal length to $f_2 = 2$ mm (figure 14(b)). The GSST2241-based varifocal metalens was fabricated, and its imaging capabilities successfully tested, obtaining high resolution, aberration-free images at the two predesigned focal planes, as shown in figure 14(c).

More recently, and following the same approach of integrating phase-change material layers within the body of high index resonators reported by de Galarreta *et al* in the NIR [68, 69, 99, 116], Leitis *et al* showed the use of thin $Ge_3Sb_2Te_6$ (GST326) layers embedded in the body of high

index cylindrical resonators, here to yield tunable optical phase-control in the MWIR [71]. Schematics and dimensions of the proposed geometry are shown in figure 14(d). It consists of a high-index germanium cylinders having two embedded GST326 layers. The device dimensions were optimised to satisfy the first Kerker condition, which can be exploited to span a 2π optical phase coverage with high efficiency in transmission. The GST326 layers were here placed in the electric displacement field maxima of the magnetic resonance, to achieve multilevel phase tuning via gradual crystallisation of the PCM. Individual cylinders were crystallised employing a pulsed laser to enable precise control of the crystallisation percentage. The phase-programming capabilities of the metasurfaces were then demonstrated via encoding of the letters 'G', 'S' and 'T' on the metasurface. Experimental maps of the corresponding phase profiles and transmittance efficiency are shown in figure 14(e), where a total phase coverage of 1.6π and an average transmittance above 50% are evident.

6. Tunable phase-change meta-devices for THz applications

The THz regime is becoming a technologically important spectral band for an increasing number of important applications, including security and defence [123, 124], biomedical sensing [123, 125], the food industry and much more [123, 126] . For instance, its non-ionizing nature allows for the attainment of x-ray-like density images without damaging living tissues, thus provides a safe source of medical detection [123]. THz radiation can also travel through materials such as dry paper and cardboard, thus could be used to detect hazardous substances by postal and delivery services [124].

In spite of its doubtless technological advantages, the THz frequency regime is still nowadays substantially limited in terms of available signal generators, detectors, and systems. In this context, metasurfaces have proved to provide a versatile platform for the manipulation of THz radiation [8, 127], thus could potentially alleviate such limitations. Furthermore, applications involving THz radiation would find many benefits if tunable and reconfigurable control of THz beams using metasurfaces were possible. In this context, to date several approaches to tunable and reconfigurable THz metasurfaces employing VO_2 have emerged over recent years, including broadband THz modulators in transmission [127, 128], multifocal THz flat lenses [129], and active switchable THz quarter-waveplates [130]. However, VO_2 being a volatile material requires for a constant heat stimulus to maintain the desired structural phase (and thus optical properties), resulting in devices with high power consumption. In addition, VO_2 transition temperatures are close to room temperature ($\sim$66 °C [127]), thus reconfigurability is strongly limited by ambient operating temperatures.

In this context, THz metasurface technologies could find strong benefits from the use of chalcogenide phase-change materials; first, because they are non-volatile in nature (thus no constant heat stimuli need to be applied to maintain a desired optical performance), and second, because they have much better thermal stabilities when compared to VO_2 (transition temperatures of GeSbTe alloys are typically around 180 °C or higher). Over the last year, some initial research work involving the use of chalcogenide phase-change metasurfaces for dynamically tunable amplitude control of THz waves has emerged [131, 132]. For instance, Pitchappa *et al* recently demonstrated the use of phase-change THz metasurfaces for multilevel, non-volatile switching with spatial and temporal selectivity [131]. As shown in figure 15(a), the device consists of periodically-arranged Al asymmetric split ring resonators lying on top of a thin GST layer on a quartz substrate. When the GST layer is amorphous, the device supports both a broadband dipole resonance and a narrowband Fano resonance, as can be appreciated in the device measured transmission spectrum shown in figure 15(b). Crystallisation of the PCM, via annealing at different temperatures, resulted in surpression of the narrowband resonance, and subsequent redshift of the dipolar resonance.

Further work on amplitude control in the THz regime was also very recently reported by Cai *et al* [132]. As shown in the device schematics in figure 15(c), the use of (symmetric) gold split-ring resonators lying on top of GST films was proposed towards narrowband amplitude modulation in transmission. When the GST is amorphous, the device supports a strong Fano-resonance at $\sim$ 0.77 THz, which can be selectively redshifted and damped via crystallisation of the PCM layer, resulting in an absolute modulation depth of 55% in transmission (figure 15(d)).

Active optical phase control employing chalcogenide phase-change metasurfaces in the THz regime is still rather unexplored, perhaps due to more complex nature of such devices, combined with the lack of available optical properties of PCMs alloys in the THz regime. In this context, the characterisation of the optical properties of different PCM alloys in the THz regime could help to identify the best compositions most suited to particular applications (for example identifying low-loss compositions needed for phase-only wavefront engineering).

7. Conclusions and future perspectives

In summary, we have here described some of the recent achievements in the use of traditional and novel PCM compositions combined with metasurfaces towards the generation of dynamically tunable meta-devices having different applications, and operating in different parts of the electromagnetic spectrum from the visible to the THz regime. The challenges arising from such a technological combination at each spectral regime have been identified, and possible research trends to overcome these challenges have been highlighted.

In particular, to our view, the visible spectrum remains the most challenging regime to work in, due to metasurface resonance damping arising from both inherent plasmonic and dielectric losses coming from metals and phase-change materials respectively. Resonance damping imposes a fundamental limit to what can be achieved with PCM-based

metasurface designs in the visible, for example in terms of the purity and efficiency of colour generation for active displays, or the amount of optical phase coverage achievable for dynamic and reconfigurable wavefront engineering. However, the recent emergence of wide bandgap, low loss PCMs such as Sb_2S_3 [73] or gallium lanthanum sulphides (GLS) [117] could enhance optical performance and facilitate the realisation of such devices.

In terms of PCM-based metasurface performance and functionalities, the NIR and MWIR/LWIR remain to date the spectral regions with perhaps the most potential, as the optical properties of conventional PCMs in such regimes are characterised by a high refractive index contrast, with low optical losses in at least one of the metastable phases. This becomes evident by looking at the variety of functionalities in the IR revisited in this manuscript, e.g. tunable amplitude *and* phase control in both transmission and reflection, when compared to other spectral regimes such as the visible or the THz, where only amplitude control has been realiably reported so far. In addition, it is expected that the development of novel low-loss PCM compositions, such as GSST, will improve even further the performance of PCM metasurfaces operating in the IR in the near future.

Turning to the THz regime, initial phase-change metasurfaces for ampltiude control have appeared for the first time over the last year, but dynamic optical phase control in the THz is still to date unexplored. The characterisation and evaluation of the optical properties of the full range of PCM compositions in the THz regime is of crucial importance to understand the possibility and limits of active PCM-based metasufaces in this important region of the spectrum.

Finally, it is undoubtedly true to say that even though tunable phase-change metasurface technology offers many attractive features, including compactness, low power consumption, high endurance and high operation speeds, for real-world applications from the visible to the THz, the technology is still at a relatively low stage of maturity and much more research and development needs to be carried out, both in terms of materials development and practicable device design. To date, a significant number of the published literature relies on numerical simulations to showcase new PCM metasurface designs [31–34, 86, 95, 109], with a smaller sub-set of concepts having been successfully fabricated and tested [27, 28, 35–38, 41–43]. Furthermore, only a few experimental demonstrations of reversible ex-situ optical switching (i.e. crystallisation and re-amorphisation) over multiple cycles can be currently found in the literature [27, 35, 38, 41], and demonstrations of *in-situ* switching of PCM metasurfaces are even rarer [41]. The ability to perform *in-situ*, pixel-by-pixel switching employing electronic methods becomes indeed a formidable engineering task, but needs to be addressed if integration of phase-change metasurfaces into real-world devices is to be achieved. The fascinating field of dynamically tunable phase-change metasurfaces will therefore benefit greatly from future research into (i) the development of practicable, electrically addressable metasurface designs with minimised PCM volumes to facilitate *in-situ* switching of the devices; and (ii) an extensive search and development of novel PCM compositions exhibiting high refractive index contrast and moderate losses in different spectral regimes.

ORCID iDs

E Gemo ⬤ https://orcid.org/0000-0001-8349-6627
C D Wright ⬤ https://orcid.org/0000-0003-4087-7467

References

[1] Darrigol O 2012 *A History of Optics: From Greek Antiquity to the Nineteenth Century* (Oxford: Oxford University Press)
[2] Smith W J 2008 *Modern Optical Engineering* (New York: McGraw-Hill)
[3] Solymar L and Shamonina E 2009 *Waves in Metamaterials* (Oxford: Oxford University Press)
[4] Yu N and Capasso F 2014 *Nat. Mater.* **13** 139–50
[5] Novotny L and Hulst N V 2011 *Nat. Photonics* **5** 83–90
[6] Alda J and Boreman G D 2017 *Infrared Antennas and Resonant Structures* (Bellingham, WA: SPIE Press)
[7] Glybovski S B, Tretyakov S A, Belov P A, Kivshar Y S and Simovski C R 2016 *Phys. Rep.* **634** 1–72
[8] He Q *et al* 2019 *Research* **2019** 1849272
[9] Nemati A, Wang Q, Hong M and Teng J 2018 *Opto-Electron. Rev.* **1** 180009
[10] Fu Y H *et al* 2011 *Adv. Funct. Mater.* **21** 3589–94
[11] Pryce I M, Aydin K, Kelaita Y A, Briggs R M and Atwater H A 2010 *Nano Lett.* **10** 4222–7
[12] Makarov S V, Zalogina A S, Tajik M, Zuev D A, Rybin M V, Kuchmizhak A A, Juodkazis S and Kivshar Y 2017 *Laser Photonics Rev.* **11** 1700108
[13] Makarov S V, Kudryashov S, Mukhin I, Mozharov A, Milichko V, Krasnok A and Belov P 2015 *Nano Lett.* **15** 6187–92
[14] Kauranen M and Zayats A V 2012 *Nat. Photonics* **6** 737–48
[15] Shirmanesh G K *et al* 2016 *Nano Lett.* **18** 2975–2963
[16] Huan Y W, Lee H W H, Sokhoyan R, Pala R A, Thyagarajan K, Han S, Tsai D P and Atwater H A 2016 *Nano Lett.* **16** 5319–25
[17] Park J, Kang J H, Liu X G and Brongersma M L 2015 *Sci. Rep.* **5** 15754
[18] Zhao Q, Kang L, Du B, Li B, Zhou J, Tang H, Liang X and Zhang B 2007 *Appl. Phys. Lett.* **90** 011112
[19] Tittl A, Mai P, Taubert R, Dregely D, Liu N and Giessen H 2011 *Nano Lett.* **11** 4366–9
[20] Duan X, Kamin S and Liu N 2017 *Nat. Commun.* **8** 14606
[21] Naorem R, Dayal G, Anantha Ramakrishna S, Rajeswaran B and Umarji A M 2015 *Opt. Commun.* **346** 154–7
[22] Savaliya P B, Thomas A, Dua R and Dhawan A 2017 *Opt. Express* **25** 23755–72
[23] Xiao S M, Chettiar U K, Kildishev A V, Drachev V, Khoo I C and Shalaev V M 2009 *Appl. Phys. Lett.* **95** 033115
[24] Wang X D, Kwon D-H, Werner D H, Khoo I-C, Kildishev A V and Shalaev V M 2007 *Appl. Phys. Lett.* **91** 143122
[25] Lewi T, Butakov N A and Schuller J A 2018 *Nanophotonics* **8** 331–8
[26] Au -Y-Y, Bhaskaran H and Wright C D 2017 *Sci. Rep.* **7** 9688
[27] de Galarreta C R *et al* 2018 *Adv. Funct. Mater.* **28** 1704993
[28] Tian J, Luo H, Yang Y, Ding F, Qu Y, Zhao D, Qiu M and Bozhevolnyi S I 2019 *Nat. Commun.* **10** 396
[29] Wuttig M and Yamada N 2007 *Nat. Mater.* **6** 824–32
[30] Wuttig M, Bhaskaran H and Taubner T 2017 *Nat. Photonics* **11** 465–76
[31] Petronijevic E and Sibilia C 2016 *Opt. Express* **21** 30411–20

[32] Cao T, Wei C and Mao L 2015 *Sci. Rep.* **5** 14666

[33] Bai W, Yang P, Huang J, Chen D, Zhang J, Zhang Z, Yang J and Xu B 2019 *Sci. Rep.* **9** 5368

[34] Zhou L, Cryan M and Klemm M 2014 *Opt. Express* **22** 24142–8

[35] Gholipour B, Zhang J, MacDonald K F, Hewak D W and Zheludev N I 2013 *Adv. Mater.* **25** 3050–4

[36] Dong W, Qiu Y, Yang J, Simpson R E and Cao T 2016 *J. Phys. Chem.* C **120** 12713–22

[37] Garcia-Cuevas Carrillo S, Trimby L, Au -Y-Y, Nagareddy V K, Rodriguez-Hernandez G, Hosseini P, Ríos C, Bhaskaran H and Wright C D 2019 *Adv. Opt. Mater.* **4** 1801782

[38] Michel A-K U, Zalden P, Chigrin D N, Wuttig M, Lindenberg A M and Taubner T 2014 *ACS Photonics* **1** 833–9

[39] Karvounis A, Gholipour B, MacDonald K F and Zheludev N I 2016 *Appl. Phys. Lett.* **109** 051103

[40] Zhu W, Yang R, Fan Y, Fu Q, Wu H, Zhang P, Shen N-H and Zhang F 2018 *Nanoscale* **10** 12054

[41] Garcia-Cuevas Carrillo S, Alexeev A M, Au -Y-Y and Wright C D 2018 *Opt. Express* **26** 25567–81

[42] Shields J, Ruiz de Galarreta C, Bertolotti J and Wright C D 2019 *E\PCOS2019* (Grenoble, France) pp 178–9

[43] Trimby L, Baldycheva A and Wright C D 2018 *Proc. SPIE* **10541** 105412B

[44] Gerislioglu B, Bakan G, Ahuja R, Adam J, Mishra Y K and Ahmadivand A 2020 *Mater. Today Phys.* **12** 100178

[45] Kim W *et al* 2016 *IEEE Int. Electron Devices Meeting (IEDM)* 16651164

[46] Bulai G *et al* 2019 *Nanomaterials* **9** 676

[47] Harmgarth N *et al* 2017 *J. Inorg. Gen. Chem.* **643** 1150–66

[48] Wang Q, Rogers E T F, Gholipour B, Wang C-M, Yuan G, Teng J and Zheludev N I 2016 *Nat. Photonics* **10** 60–65

[49] Ding F, Yang Y and Bozhevolnyi S I 2019 *Adv. Opt. Mater.* **7** 1801709

[50] Hail C U, Michel A-K U, Poulikakos D and Eghlidi H 2019 *Adv. Opt. Mater.* **7** 1801786

[51] Hudgens S and Jhonson B 2004 *MRS Bull.* **29** 829–32

[52] Zhang Y *et al* 2019 *Nat. Commun.* **10** 4279

[53] Shportko K, Kremers S, Woda M, Lencer D, Robertson J and Wuttig M 2008 *Nat. Mater.* **7** 653–8

[54] Raoux S and Wuttig M 2009 *Phase Change Materials* (Berlin: Springer)

[55] Siegel J, Gawelda W, Puerto D, Dorronsoro C, Solis J, Afonso C N, de Sande J C G, Bez R, Pirovano A and Wiemer C 2008 *J. Appl. Phys.* **103** 023516

[56] Siegel J, Schropp A, Solis J and Afonso A N 2004 *Appl. Phys. Lett.* **84** 2250

[57] Kohary K and Wright C D 2011 *Appl. Phys. Lett.* **98** 223102

[58] Kim D-H, Merget F, Laurenzis M, Bolivar P H and Kurz H 2005 *J. Appl. Phys.* **97** 083538

[59] Kooi B J and Wuttig M 2020 *Adv. Mater.* **32** 1908302

[60] Kolobov A V and Tominaga J 2012 *Chalcogenides* (Berlin: Springer)

[61] Redaelli A 2018 *Phase Change Memory. Device Physics, Reliability and Applications* (Berlin: Springer)

[62] Athmanathan A *et al* 2016 *IEEE J. Emerging Sel. Top. Circuits Syst.* **6** 87–100

[63] Li X *et al* 2019 *Optica* **6** 1–6

[64] Rios C, Stegmaier M, Hosseini P, Wang D, Scherer T, Wright C D, Bhaskaran H and Pernice W H P 2015 *Nat. Photonics* **9** 725–32

[65] Gemo E, Carrillo S G-C, De Galarreta C R, Baldycheva A, Hayat H, Youngblood N, Bhaskaran H, Pernice W H P and Wright C D 2019 *Opt. Express* **27** 24724–37

[66] Rios C, Hosseini P, Wright C D, Bhaskaran H and Pernice W H P 2014 *Adv. Mater.* **26** 1372–7

[67] Michel A-K U *et al* 2013 *Nano Lett.* **13** 3470–5

[68] de Galarreta C R *et al* 2019 arXiv:1901.04955

[69] de Galarreta C R, Sinev I, Alexeev A M, Trofimov P, Ladutenko K, Garcia-Cuevas Carrillo S, Gemo E, Baldycheva A, Bertolotti J and David Wright C 2020 *Optica* **7** 476–84

[70] Paniagua-Dominguez R, Ha S T and Kuznetsov A I 2019 *Proc. IEEE* **108** 749–71

[71] Leitis A *et al* 2020 *Adv. Mater.* **30** 1910259

[72] Shalaginov M Y *et al* 2019 arXiv:1911.12970

[73] Dong W, Liu H, Behera J K, Lu L, Ng R J H, Sreekanth K V, Zhou X, Yang J K W and Simpson R E 2019 *Adv. Funct. Mater.* **29** 1806181

[74] Yang B, Cheng H, Chen S and Tian J 2019 *Mater. Chem. Frontiers* **5** 750–61

[75] Hedayati M K and Elbahri M 2017 *Plasmonics* **12** 1463–79

[76] Kim I, Yoon G, Jang J, Genevet P, Nam K T and Rho J 2018 *ACS Photonics* **5** 3876–95

[77] Clausen J S, Højlund-Nielsen E, Christiansen A B, Yazdi S, Grajower M, Taha H, Levy U, Kristensen A and Mortensen N A 2014 *Nano Lett.* **14** 4499–504

[78] Shang S *et al* 2017 *ACS Nano* **11** 4445–52

[79] Proust J *et al* 2016 *ACS Nano* **10** 7761–7

[80] Koirala I, Lee -S-S and Choi D-Y 2018 *Opt. Express* **26** 18320–30

[81] Hosseini P, Wright C D and Bhaskaran H 2014 *Nature* **511** 206–11

[82] Rios C, Hosseini P, Taylor R A and Bhaskaran H 2016 *Adv. Mater.* **28** 4720–6

[83] Ji H-K, Tong H, Qian H, Hui Y-J, Liu N, Yan P and Miao X-S 2016 *Sci. Rep.* **6** 39206

[84] Yun M, Ramakrishnegowda N, Park D-S and Bhatnagar A 2018 *Appl. Phys. Lett.* **113** 071901

[85] Vermeulen P A, Yimam D T, Loi M A and Kooi B J 2019 *J. Appl. Phys.* **125** 193105

[86] Cao T, Wei C-W, Simpson R E, Zhang L and Cryan M J 2015 *Sci. Rep.* **4** 3955

[87] Broughton B *et al* 2017. *Society for Information Display Int. Symp.* **48** 546–9

[88] Gholipour B, Karvounis A, Yin J, Soci C, MacDonald K F and Zheludev N I 2018 *NPG Asia Mater.* **10** 533–9

[89] Hu X L *et al* 2017 *J. Appl. Phys.* **131** 153105

[90] Aieta F, Genevet P, Kats M A, Yu N, Blanchard R, Gaburro Z and Capasso F 2012 *Nano Lett.* **12** 4932–6

[91] Sun S *et al* 2012 *Nano Lett.* **12** 6223–9

[92] Zheng G, Mühlenbernd H, Kenney M, Li G, Zentgraf T and Zhang S 2015 *Nat. Nanotechnol.* **10** 308–12

[93] Garcia-Cuevas S, Nash G R, Hayat H, Cryan M J, Klemm M, Bhaskaran H and Wright C D 2016 *Opt. Express* **24** 13563–73

[94] Pogrebnyakov A V, Bossard J A, Turpin J P, Musgraves J D, Shin H J, Rivero-Baleine C, Podraza N, Richardson K A, Werner D H and Mayer T S 2018 *Opt. Express* **8** 2264–75

[95] Cao T, Zheng G, Wang S and Wei C 2015 *Opt. Express* **23** 18029–39

[96] Samson Z L, MacDonald K F, De Angelis F, Gholipour B, Knight K, Huang C C, Di Fabrizio E, Hewak D W and Zheludev N I 2010 *Appl. Phys. Lett.* **96** 143105

[97] Chen Y G, Kao T S, Ng B, Li X, Luo X G, Luk'yanchuk B, Maier S A and Hong M H 2013 *Opt. Express* **21** 13691–8

[98] Chen Y, Li X, Maier S A and Hong M 2015 *Opt. Express* **3** 54–57

[99] De Galarreta C R, Alexeev A, Bertolotti J and Wright C D 2018 *IEEE Int. Symp. Circuits Syst.* 18242933

[100] Xu P, Zheng J, Doylend J K and Majumdar A 2019 *ACS Photonics* **6** 553–7

[101] Stegmaier M, Rios C, Bhaskaran H, Wright C D and Pernice H P W 2016 *Adv. Opt. Mater.* **5** 1600346

[102] Feldmann J, Youngblood N, Li X, Wright C D, Bhaskaran H and Pernice W H P 2020 *IEEE J. Sel. Top. Quantum Electron.* **26** 8301807

[103] Feldmann J, Stegmaier M, Gruhler N, Ríos C, Bhaskaran H, Wright C D and Pernice W H P 2017 *Nat. Commun.* **8** 1256

[104] Feldmann J, Youngblood N, Wright C D, Bhaskaran H and Pernice W H P 2019 *Nature* **569** 208–14

[105] Farmakidis N, Youngblood N, Li X, Tan J, Swett J L, Cheng Z, Wright C D, Pernice W H P and Bhaskaran H 2019 *Sci. Adv.* **5** eaaw2687

[106] Faneca J, Trimby L, Zeimpekis I, Delaney M, Hewak D W, Gardes F Y, Wright C D and Baldycheva A 2020 *Opt. Express* **28** 16394–406

[107] Faneca J, Dominguez Bucio T, Gardes F Y and Balducheva A 2020 *Appl. Phys. Lett.* **116** 093502

[108] Forouzmand A and Mosallaei H 2018 *Opt. Express* **26** 17948–63

[109] Chu C H *et al* 2016 *Laser Photonics Rev.* **10** 986–94

[110] Vollmer M and Mollmann K-P 2010 *Infrared Thermal Imaging: Fundamentals, Research and Applications* (New York: Wiley)

[111] Sherott M C, Hon P W C, Fountaine K T, Garcia J C, Ponti S M, Brar V W, Sweatlock L A and Atwater H A 2017 *Nano Lett.* **17** 3027–34

[112] Zhang S *et al* 2016 *Opt. Express* **24** 18024–34

[113] Zhu Y *et al* 2018 *Light Sci. Appl.* **7** 67

[114] Tittl A, Leitis A, Liu M, Yesilkoy F, Choi D-Y, Neshev D N, Kivshar Y S and Altug H 2018 *Science* **360** 6393

[115] Rodrigo D *et al* 2018 *Nat. Commun.* **9** 2160

[116] Ruiz de Galarreta Fanjul C 2019 Reconfigurable phase-change optical metasurfaces: novel design concepts to practicable devices *PhD Thesis* University of Exeter

[117] Trimby L 2019 Phase-change meta-devices for tuneable bandpass filtering in the infrared *PhD Thesis* University of Exeter

[118] Mao L and Cao T 2016 *J. Sci.: Adv. Mater. Devices* **1** 393–9

[119] Qu Y, Li Q, Du K, Cai L, Lu J and Qiu M 2017 *Laser Photonics Rev.* **11** 1700091

[120] Rudé M, Mkhitaryan V, Cetin A E, Miller T A, Carrilero A, Wall S, de Abajo F J G, Altug H and Pruneri V 2016 *Adv. Opt. Mater.* **4** 1060–6

[121] Yin X *et al* 2017 *Light Sci. Appl.* **6** e17016

[122] Decker M *et al* 2015 *Adv. Opt. Mater.* **3** 813–20

[123] Jones I, Rainsford T J, Mickan S P and Abbot D 2005 *Proc. SPIE* **6038** 603811

[124] Choi M K, Bettermann A and van der Wiede D W 2004 *Phil. Trans.* A **362** 347–9

[125] Siegel P H 2004 *IEEE Trans. Microwave Theory and Tech.* **52** 2438–47

[126] Manthanker S K, Weckler P R and Wang N 2013 *Trans. Am. Soc. Agric. Biol. Eng.* **56** 1213–26

[127] Al-Naib I and Withayachumnakul W 2017 *J. Infrared Millimeter Terahertz Waves* **38** 1067–84

[128] Zhou G *et al* 2017 *Opt. Express* **25** 17322–8

[129] Kargar R, Rouhi K and Abdolali A 2020 *Opt. Commun.* **462** 125331

[130] Wang D, Zhang L, Gu Y, Mehmood M Q, Gong Y, Srivastava A, Jian L, Venkatesan T, Qiu C-W and Hong M 2015 *Sci. Rep.* **5** 15020

[131] Pitchappa P, Kumar A, Prakash S, Jani H, Venkatesan T and Singh R 2019 *Adv. Mater.* **31** 1808157

[132] Cai L *et al* 2019 *10th Int. Conf. of Materials for Advanced Technologies (ICMAT)* Marina Bay Sands, Singapore